

Roadmap and direction towards high performance MoS₂ hydrogen evolution catalysts

Yang Cao

Department of Energy and Resources Engineering, College of Engineering, Peking University, Beijing, 100871 P. R. China.

Abstract

MoS₂ is a typical 2D transition metal dichalcogenide, and have exhibit superior electrocatalytic HER activity. The MoS₂'s HER catalysis was developed 15 years ago, various nanofabrication strategies are applied to boost the performance. It is promising that MoS₂ would take place of Pt in HER catalysis. Various active catalytic sites, including edge, vacant, basal plane, *etc.* are developed and the catalytic performance were compared. Hybrid composition were developed, like modification with atoms, clusters, loading on substrates were developed. We make a summary on HER mechanisms varies with active sites and operation solutions. MoS₂ synthesis, characterization, HER performance, mechanisms, to make a holistic understanding on the interplay between the structure, chemistry, HER performance, and mechanism. It is believed that the review will help researchers to get a better understanding on MoS₂'s superior HER performance, and provide a wealth of catalyst tool box to promote next-generation catalysts development.

Main text

Hydrogen energy is perceived as the most promising clean energy without any carbon emission like CO₂. For the greenhouse effect is becoming increasingly serious issue caused by large application of fossil fuel, hydrogen fuel is an innovative solution and show great potential in resolute carbon emission. Electrocatalytic water splitting is the best achievable approach nowadays for achieving large amount of H₂.

MoS₂ are facile, stable, non-toxic, affordable materials with reasonable price, and have exhibit its superior potential in catalysis, sensing, opt electrochemical, environmental relate application¹, *etc.* Modification of MoS₂ materials has been widely applied for adjusting and formulate the relative performance in certain application field. MoS₂ is a typical transition metal dichalcogenide² (TMD) compound with a two-dimensional S-Mo-S tri-atom layer structure.

MoS₂ is predicted to be a promising substitute catalyst for platinum 15 years ago³. While pristine MoS₂ shows low electrocatalysis performance, via vacancies engineering, phase engineering, heterojunction engineering, hetero-atom doping strategies, the catalytic active sites quantities are elevated and catalysis performance is magnitude improved.

We summarize on MoS₂ synthesis, characterization, HER performance, mechanisms, to make a holistic understanding on the interplay between the structure, chemistry, HER performance, and

mechanism, which will give directions to elevate other electrochemical reaction by MoS₂.

Structural, fundamental physical and chemical properties of MoS₂:

MoS₂ has been applied as lubricant materials at industrial level in alleviate worn out phenomenon⁴⁻⁵. Generally, two-dimensional MoS₂ exist 4 main crystal structure, which are 1H, 1T, 2H, 3R⁶. Among them, 1H MoS₂ is the most stable phase. MoS₂ is composed with S-Mo-S trilayer atoms, whereas the layers are weakly coupled and the interlayer space is around 3 Å between the adjacent two layers. 2H, 1T phase of MoS₂ are composed with hexagonally Mo atoms or tetragonal Mo atoms, and they are semiconducting or metallic, respectively. Which is fascinating to chemist and physicist is the adjustable structure and correlate unique electronic properties, catalytic activities. MoS₂ exhibit a wealthy of quantum physics like quantum spin Hall insulator and superconducting states⁷ (Figure 1). It has been posited that the favored crystal phase can be easily switched by regulate the electron filling of d orbitals⁷⁻⁸.

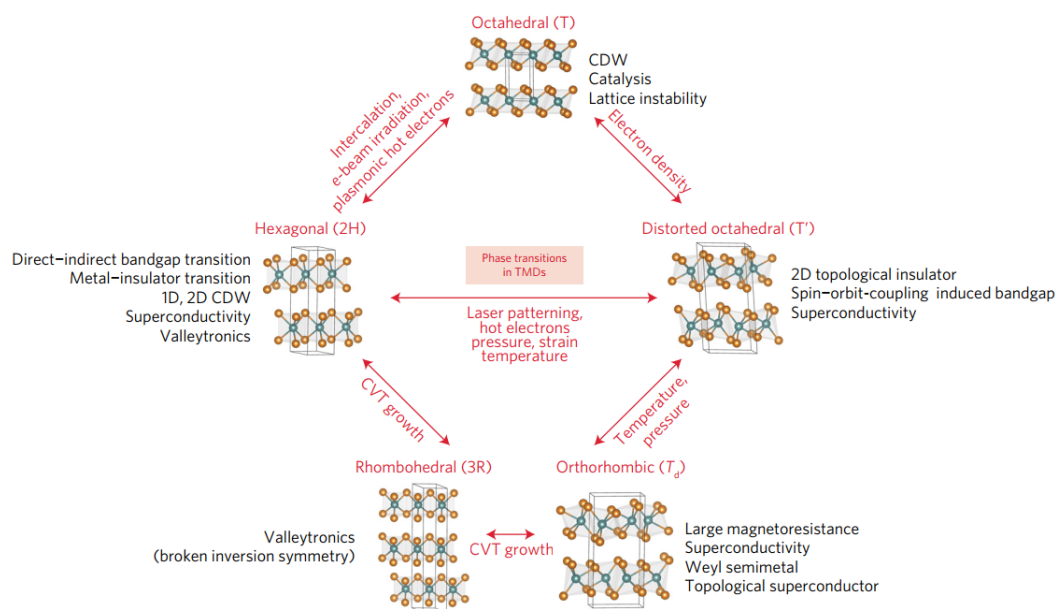


Figure 1. Transition metal dichalcogenides compound phase transition and correlation between different phase and physics⁷ (Copyright 2017, Nature Publishing Group).

MoS₂'s structure is closely related to its electronic structure. As depicted in Figure 2a, pristine MoS₂'s structure trigonal prismatic (Figure 2a, b), but 1T phase MoS₂ is octahedral⁷ (Figure 2a, c). The natural bulky MoS₂ exhibit as semiconducting 2H phase with an indirect band gap of 1.3 eV. when the thickness is reduced to around 100 nm, the band energy is elevated to 1.6 eV caused by quantum confinement effect. When the thickness is reduced to monolayer, the band gap is transformed from indirect to direct with the predict theoretical band gap ~1.9 eV. The disordered 1T' phase (partly metallic 1T phase) is still semiconductor with a band gap close to zero (0.1 eV)⁹. When MoS₂ is 1T phase, MoS₂ is totally changed to metallic without any band-gap energy. As depicted in Figure 3, when convert from 2H towards 1T phase, MoS₂ lattice structure and electronic structure evolved along with electron injection, electron rearrangement, charge loss¹⁰. And the

resultant 1T MoS₂ can be reversed to pristine 2H MoS₂ by charge rearrangement. Suenaga *et. al.* traced the phase conversion from 2H to 1T using TEM and find that process undergo atomic glide (Figure 3b)¹¹, and α intermediate phase were identified under MoS₂ monolayer. During phase conversion, some other metastable distorted phase were also formed (1T', 1T'', 1T''')¹². In these metastable phases, zigzag Mo-Mo chains and dimerization Mo (1T'') or trimerization Mo (1T''') atoms with closer Mo-Mo distance were found¹³.

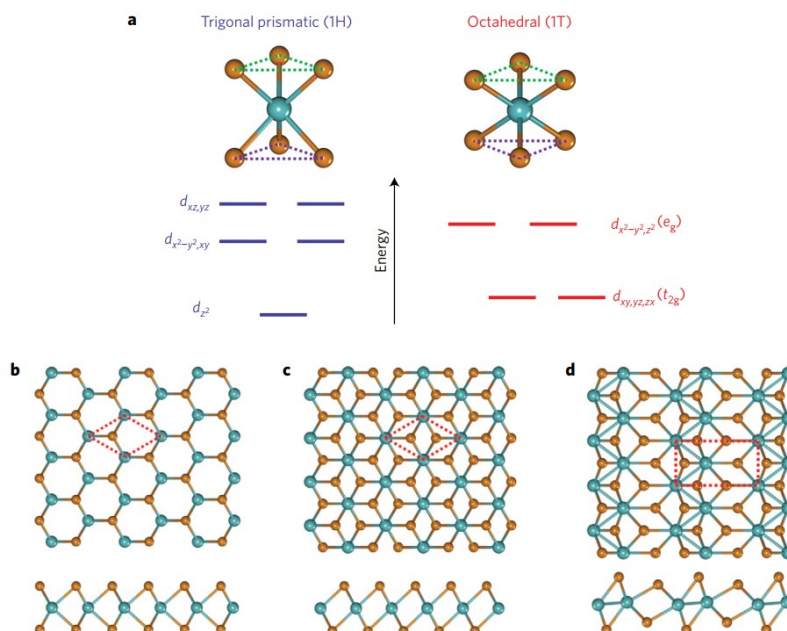


Figure 2. Structures of single-layer TMDs. **a**, Schematic images of 1H and 1T lattice symmetries and energy levels of *d*-orbital electrons induced by the crystal field. **b–d**, Top and side structures of 1H (**b**), 1T (**c**) and distorted 1T or 1T' (**d**). Blue spheres represent transition metals, and orange spheres denote chalcogen elements⁷ (Adapted with permission from ref. 7. Copyright 2017, Nature Publishing Group).

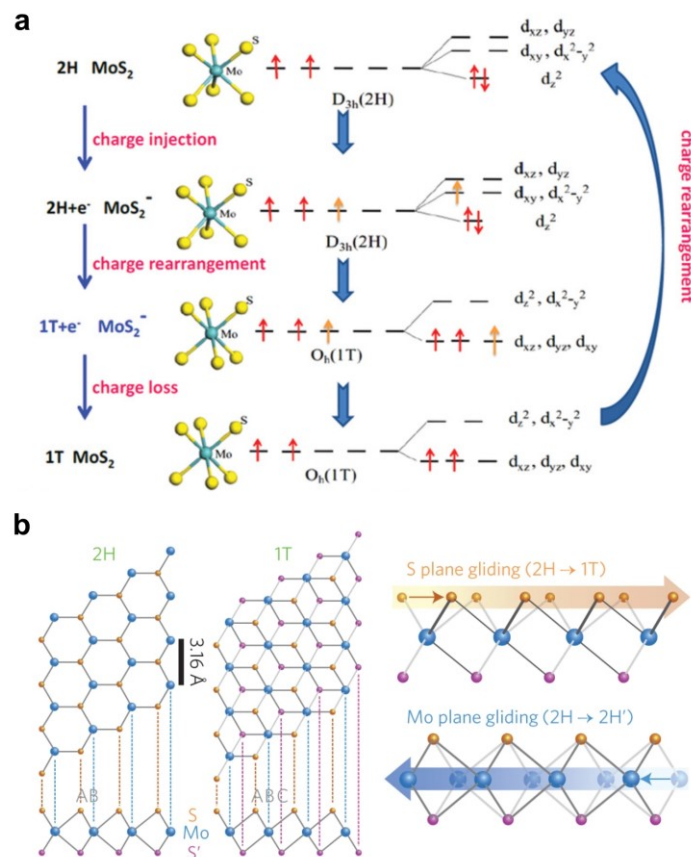


Figure 3. Phase transition between 1T and 2H mechanism based on the crystal field theory¹¹. Schematic models of single-layered MoS₂ with 2H (a) (Adapted with permission from ref. 10. Copyright 2019, Wiley-VCH Verlag GmbH & Co. KGaA, Weinheim) and 1T (b) phases in basal plane and cross-section views (Adapted with permission from ref. 11. Copyright 2014, Nature Publishing Group)

Determination on MoS₂'s structure and the relative characterization:

Determination of the morphology, structure and phase are focal points for MoS₂ materials, correlate the catalytic performance with the structure, identify the catalytic active site. The structural represent direct relationship with MoS₂'s HER catalytic performance, structure examination is a vital issue for understanding and design stable MoS₂ catalyst with high performance.

Powdered XRD characterization:

By examine the XRD data, the crystallization behavior, phase constitution, crystal lattice information of the MoS₂ can be arrived. As depict in Figure 4a, 2H and 1T' would be distinguished for the (002) peak position. Some displaced 1 T phase (1T'', 1T''') that difficult to identify as well as uncommon 3R phase can be indexed with the XRD results (Figure 4b, c)¹⁴⁻¹⁷. What's more, as depicted in Figure 5, (002) lattice plane (around 8~13°) is often applied to estimate MoS₂'s the interlayer distance by Bragg's law¹⁸.

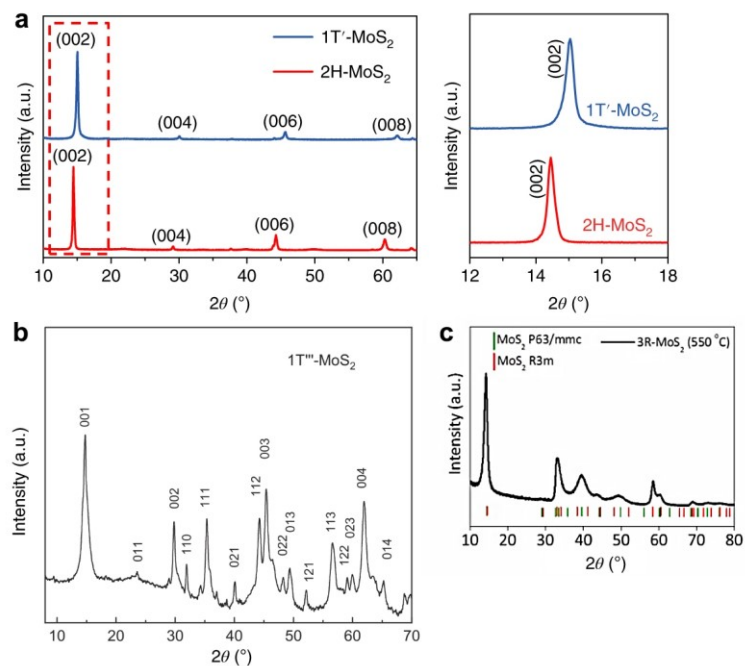


Figure 4. XRD patterns of (a) 1T'-MoS₂ crystals and 2H-MoS₂ crystals¹⁶ (Adapted with permission from ref. 16. Copyright 2018, Nature Publishing Group) (b) 1T'''-MoS₂¹⁵ (Adapted with permission from ref. 15. Copyright 2019, American Physical Society.) (c) 3R phase MoS₂¹⁷ (Adapted with permission from ref. 17. Copyright 2019, Royal Chemical Society.)

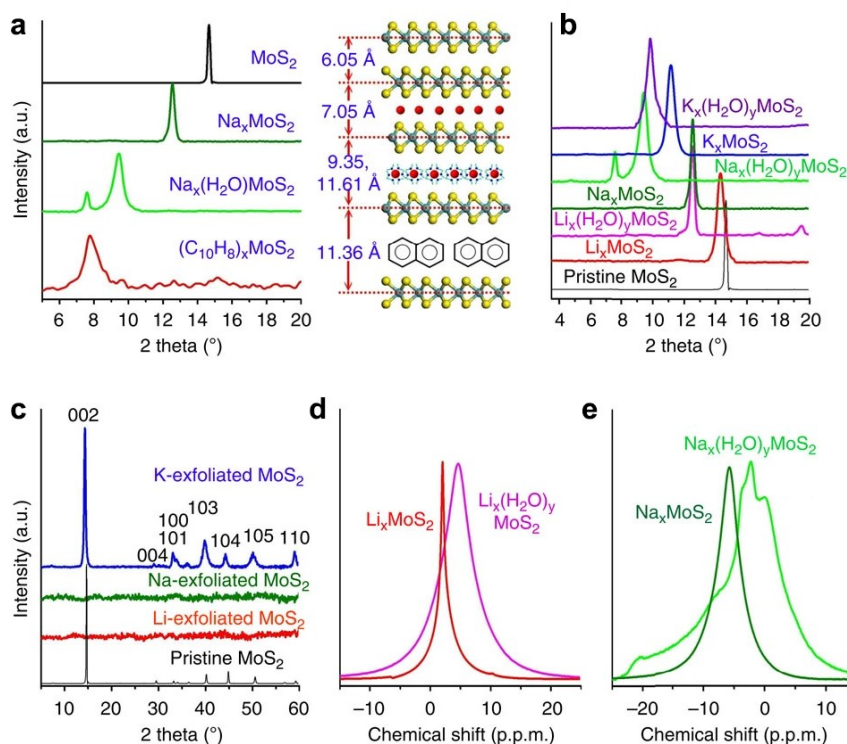


Figure 5. (a) XRD pattern and schematic of pristine MoS₂, Na-intercalated MoS₂, after exposure of Na-intercalated MoS₂ to the ambient for 3 days, exfoliated-and-restacked naphthalene-intercalated MoS₂. (b) Li-, Na- and K-intercalated MoS₂, after exposure of intercalated sample to the ambient for 3 days. (c) Li-, Na- and K-exfoliated MoS₂ without any annealing. (d) Solid-state ⁷Li NMR spectra of Li_xMoS₂ and Li_x(H₂O)_yMoS₂, (e) Solid-state ²³Na NMR spectra of Na_xMoS₂ and Na_x(H₂O)_yMoS₂

$\text{Na}_x(\text{H}_2\text{O})_y\text{MoS}_2$ ¹⁸. (Adapted with permission from ref. 18. Copyright 2014, Nature Publishing Group)

UV-Vis spectra and photo luminance characterization:

It has been determined that 2H MoS₂'s absorption at around 600 and 670 nm (Figure 6a) are attribute to energy splitting from valance band and spin-orbit coupling¹⁹. 1T MoS₂ do not show any absorption ~600 nm for it belongs to metallic phase²⁰. UV-Vis spectra can reflect on the structure of MoS₂, *i.e.* in Figure 6b, MoS₂ quantum dot shows strong absorption at ~300 nm, which is distinct from nanosheet or bulk MoS₂²¹. MoS₂ nanosheet and MoS₂ bulk display much stronger absorption in visible light region.

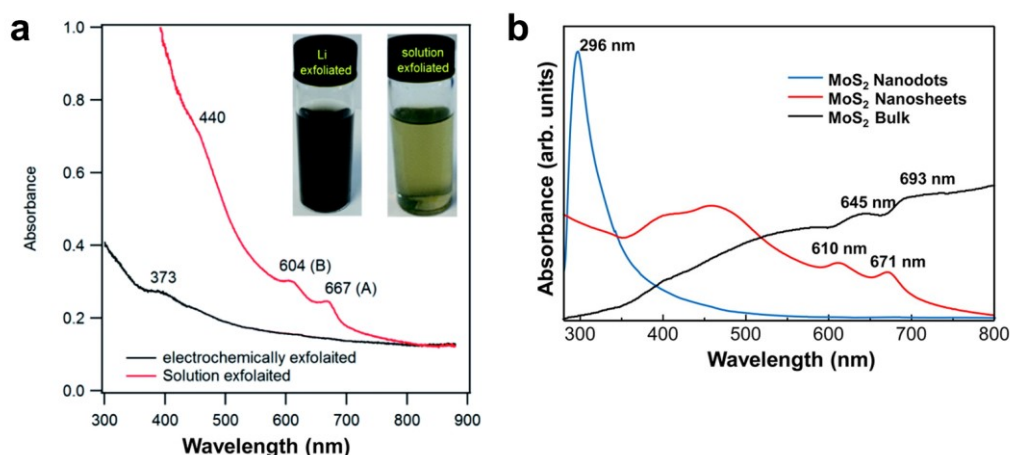


Figure 6. Optical absorption spectrum of MoS₂ (a) MoS₂ (Li exfoliated MoS₂: metallic phase, solution exfoliated MoS₂: semiconducting phase) dispersion in the mixture of water and isopropanol (1:1)²⁰. (Adapted with permission from ref 20, Copyright 2017, Royal Chemical Society.) (b) MoS₂ nanodots, nanosheets, and bulk materials²¹. (Adapted with permission from ref 21. Copyright 2016, American Chemical Society.)

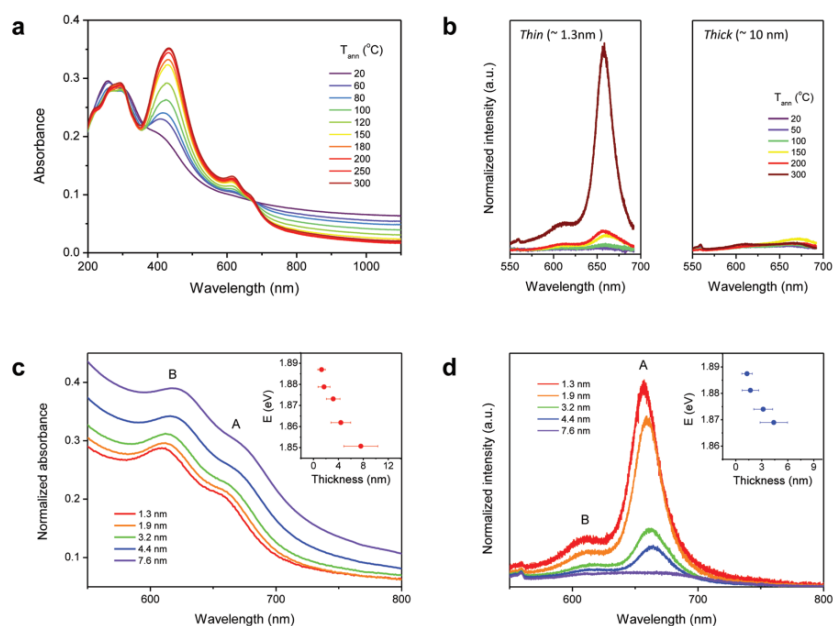


Figure 7 (a) Absorption and (b) photoluminescence spectra of MoS₂ thin films annealed at various temperatures. (c) Absorption and (d) photoluminescence spectra of MoS₂ thin films with average thicknesses ranging from 1.3 to 7.6 nm²². (Adapted with permission from ref 22. Copyright 2011, American Chemical Society)

The photo luminance intensity and excitation position are sensitive to the structure and thickness of MoS₂, few layered MoS₂ has been exfoliated and studied²². As depicted in Figure 7, when the thickness of MoS₂ is increased from 1.3 nm to 7.6 nm, visible light absorption is elevated, while photoluminescence is decayed, when MoS₂ is reached to 7.6 nm, the photoluminescence vanished.

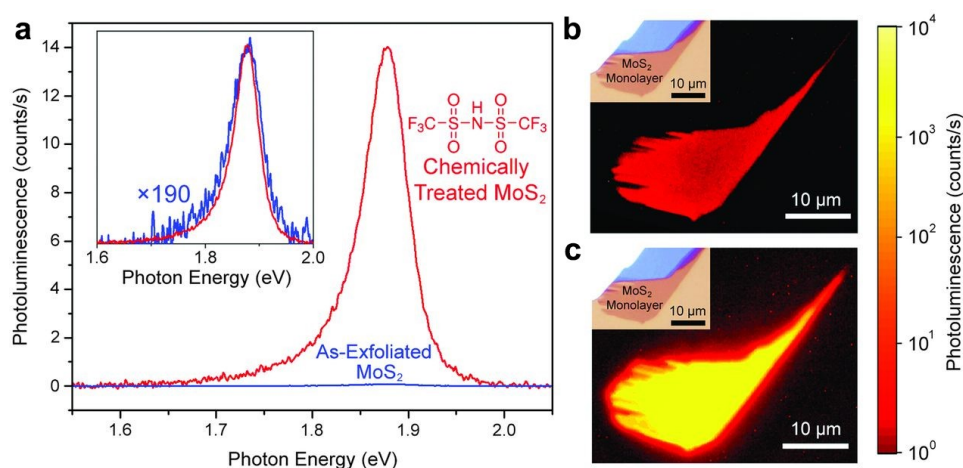


Figure 8 (a) PL spectrum for both the as-exfoliated and TFSI-treated MoS₂ monolayers measured at an incident power of $1 \times 10^{-2} \text{ W cm}^{-2}$. The inset shows normalized spectra. (b) PL images of a MoS₂ monolayer before (b) and after treatment (c). Insets show optical micrographs²³. (Adapted with permission from ref 23. Copyright 2015, American Association for the Advancement of Science)

Another study shows that the MoS₂'s poor photo luminance can be fine-tuned by surface organic molecule modification strategies. As depicted in Figure 8, the pristine photo luminance of MoS₂ display poor luminescence quantum yield (0.01 % to 6 % in the available studies) for large amount of defects, whereas nearly 100 % quantum yield were achieved by surface modification with TFSI molecules²³. What's more, chemical doping (F₄TCNQ) method have been developed to tune the photo luminance performance of monolayer MoS₂²⁴.

XPS characterization:

XPS spectra is sensitive to the chemical environment, and MoS₂'s crystal phase constitution can be determined by Mo 3d binding energy spectra²⁵. As depicted in Figure 9(a-b), Hofmann *et. al.* study Mo 3d and S 2p spectra of 2H, 1T, amorphous MoS₂ changes before and after HER reaction, the XPS spectra show that Mo 3d and S 2p spectra of 2H MoS₂ unchanged, while Mo 3d and S 2p spectra shifted in 1T and amorphous MoS₂²⁶.

As depicted in Figure 9(c-f), McDowell *et. al.* made a detailed study on the interface of MoS₂ reaction with various metals (Li, Ge, Ag) on the interface by XPS characterization strategies, on the XPS study on MoS₂'s reaction under variant *in-situ* chemical deposit reaction²⁷, reaction between MoS₂ and Li, Ag, Ge were depicted. The XPS peak shift were attributed to interface reaction during metal deposition. To fitting Mo 3d spectra to multiple peaks corresponding to different phases, and get a brief phase constitution of 1T and 2H phase²⁸.

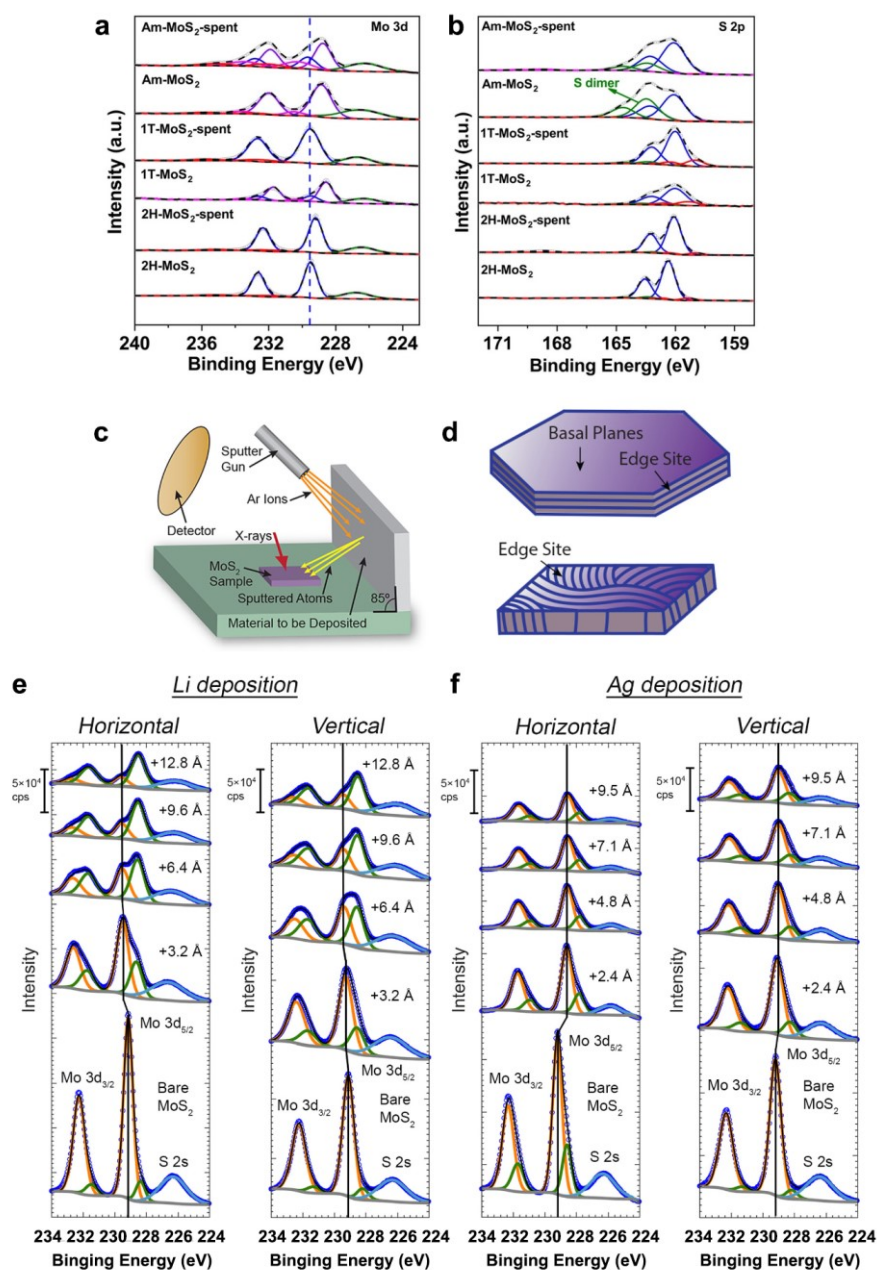


Figure 9 (a) X-ray photoemission spectra of Mo 3d (a) and S 2p (b) before and after (spent) operando XAS measurements²⁶ (c) Schematic of a single MoS₂ crystal showing the position of basal planes and edge sites. (d) the layers are aligned along the electron beam as shown in the schematic below. (e) Evolution of Mo 3d peaks with progressive deposition of Li (e) and Ag (f)²⁷. (Adapted with permission from ref. 26-27. Copyright 2019, Wiley-VCH Verlag GmbH & Co. KGaA, Weinheim)

TEM characterization:

MoS₂ can be visualized to identify the crystal phase by TEM and attribute the TEM patterns to distinct crystal lattice. As depicted in Figure 10, in a tri-phase MoS₂ material, 1T, 2H, 3R lattice region in a single MoS₂ nanosheet can be identified by high resolute TEM²⁹. In a typical literature,

the Re doped single-layer MoS₂'s phase engineering between 2H and 1T were visualized¹¹. What's more, grain boundaries and defects can be discerned in high resolute TEM. Applying to an environmental TEM, MoS₂'s phase conversion can be monitored. As depicted in Figure 11, J. Hong *et. al.* explored the atomic defects in MoS₂ monolayer, and found 5 types of antisite site by HADDF model TEM, successfully make an irrefutable proof on MoS₂'s defective structure³⁰. And the electronic structures of different antisite defects were studied.

Distort 1T phase display zigzag metal chain attract much eyes for its unique properties: enhanced electrocatalytic performance, superconductivity, *etc*³¹. The structural relationship was clearly depicted by Zhu *et. al.*³²

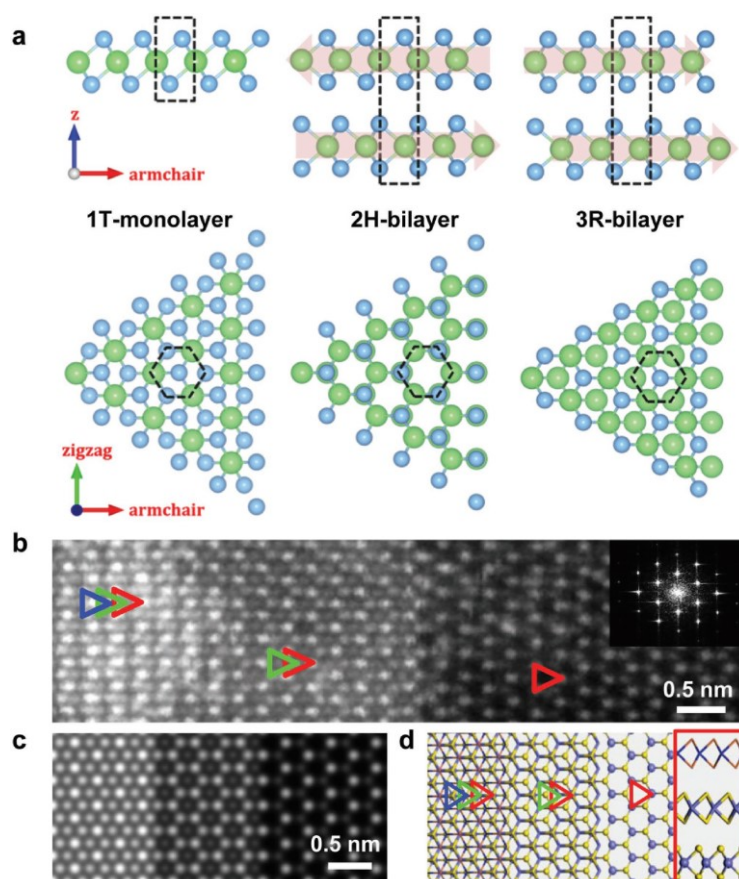


Figure 10. Schematic view of MoS₂ different phases and characterization of 3R phase MoS₂. (a) (Left to right): 1T, 2H phase (hexagonal symmetry), and 3R phase (rhombohedral symmetry) of MoS₂. (b) Atomic resolution STEM-ADF image of monolayer, bilayer, and trilayer 3R MoS₂ (from right to left) overlaid with corresponding diffraction pattern of 3R crystal. (c) Simulated image of STEM-ADF image of MoS₂. (d) Structure model corresponds to (b), which clearly shows the structure of different phase MoS₂. The picture in red frame shows the side view of monolayer MoS₂²⁹. (Adapted with permission from ref. 29. Copyright 2017, Wiley-VCH Verlag GmbH & Co. KGaA, Weinheim)

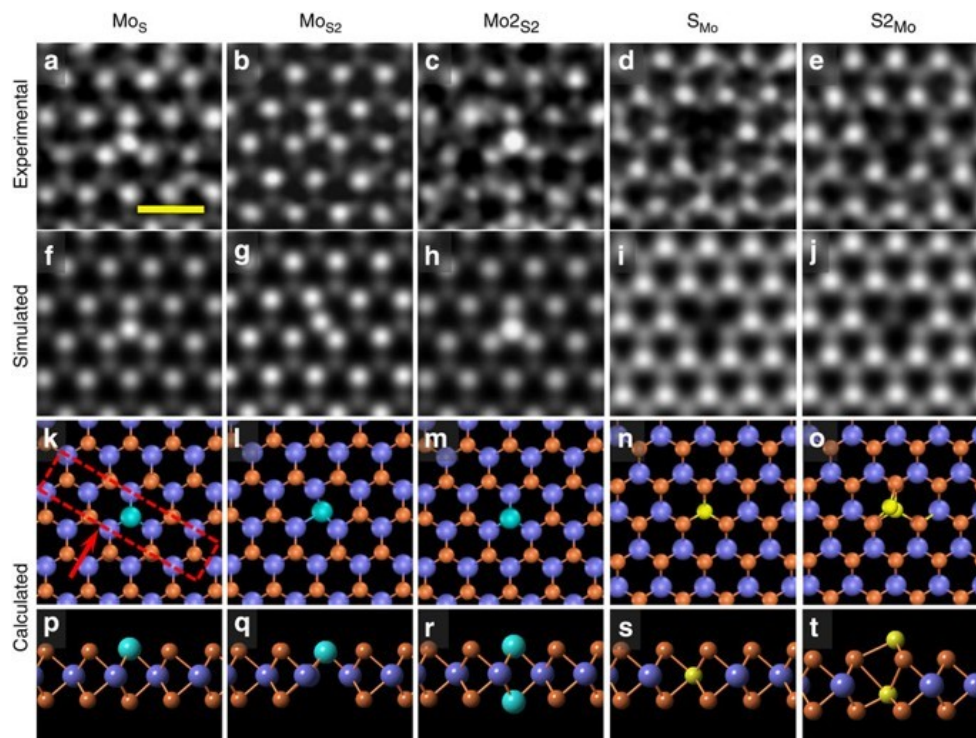


Figure 11. Different Mo antisite defect site³⁰. (Adapted with permission from ref. 30. Copyright 2015, Nature Publishing Group)

Raman spectra characterization:

Raman spectra are widely applied to distinguish lattice structure³¹, layer thickness of MoS₂³³. 2H phase and 1T phase Raman spectra are distinct different and easily compared³¹. Hong Li *et. al.* established a detailed study on the MoS₂'s Raman spectra with different layer (1~4 layer), and Raman spectra were characterized with various laser lines (which are centered at 325, 488, 514.5, 532, 632.8 nm).³³ The relationship between the coupling of electronic transitions and the phonons were studied. The *operando* Raman spectra of amorphous MoS₂ were studied in detail by Yeo *et. al.*³⁴.

As depicted in Figure 12, tip-enhanced Raman spectroscopy (TERS) has been developed and successfully applied to make a closer focus on the localized MoS₂'s atomic structure, especially on the edge site structure which was identified as the catalytic site before³⁵.

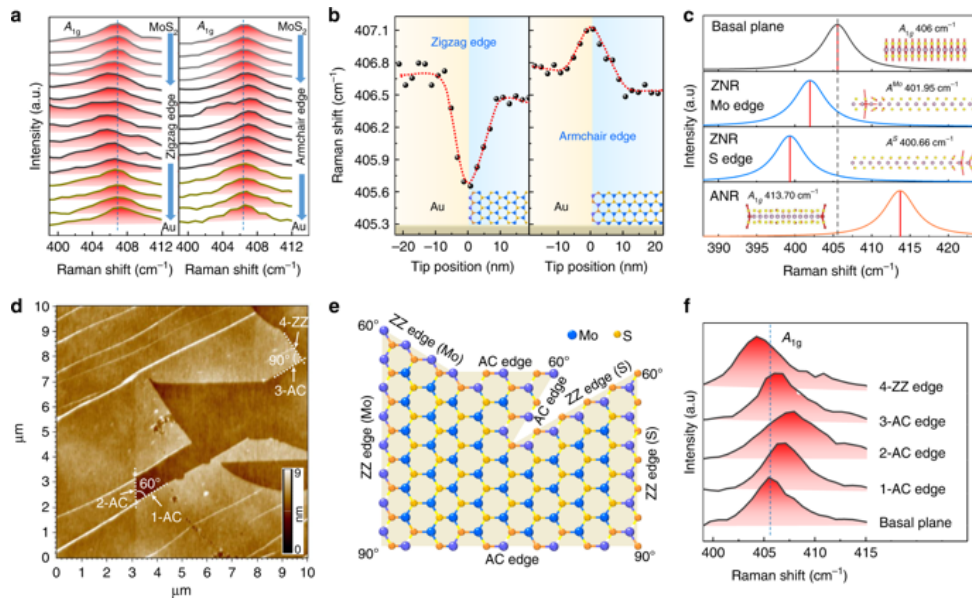


Figure 12. Effect of the edge structure on the peak position of the Raman A_{1g} mode. (a) Typical line-trace TERS spectra of the zigzag edge (left panel) and armchair edge (right panel) in the spectral range of the A_{1g} mode. (b) Plots of peak position with the tip position. (c) Calculated Raman spectra and lattice vibration of the basal plane, zigzag nanoribbon (ZNR, with a width of 3.59 nm) localized at the Mo and S edges, and armchair nanoribbon (ANR, with a width of 2.05 nm). (d) AFM image of a mechanically exfoliated 1 L MoS₂ with different edge angles on an Au substrate. (e) Illustration of the relationship between angles and edge structures of zigzag (ZZ) and armchair (AC) in 2 H MoS₂. (f) TERS spectra of four edges in the spectral range of the A_{1g} mode marked in (d)³⁵. (Adapted with permission from ref. 35. Copyright 2019, Nature Publishing Group)

X-ray absorption spectroscopy:

As depicted in Figure 13, the MoS₂ with 1T, 2H, as well as amorphous structures under HER were characterized, and the stability, bonding structure changes were clearly compared²⁶.

Zelege *et. al.* applied XAS to study the interaction between MoS₂ and the carbonized polyacrylonitrile substrate, and find that low coordinating Mo catalytic site is responsible for higher catalytic performance³⁶.

In-situ X-ray absorption spectroscopy (XAS) has been widely applied in measurement of the nano catalysts' oxidation states, local environments during the real reaction conditions to footprint the changes in the catalysis process³⁷. Hoffman *et. al.* make a detailed study on 1T, 2H, amorphous MoS₂ atomic bonding and electronic structures by utilizing Mo K edge XANES and Mo K-edge Fourier transform EXAFS (k²-weighted), the results clearly show that 1T and amorphous MoS₂ display short Mo-S bond than 2H MoS₂, which may afford for the better HER performance³⁷.

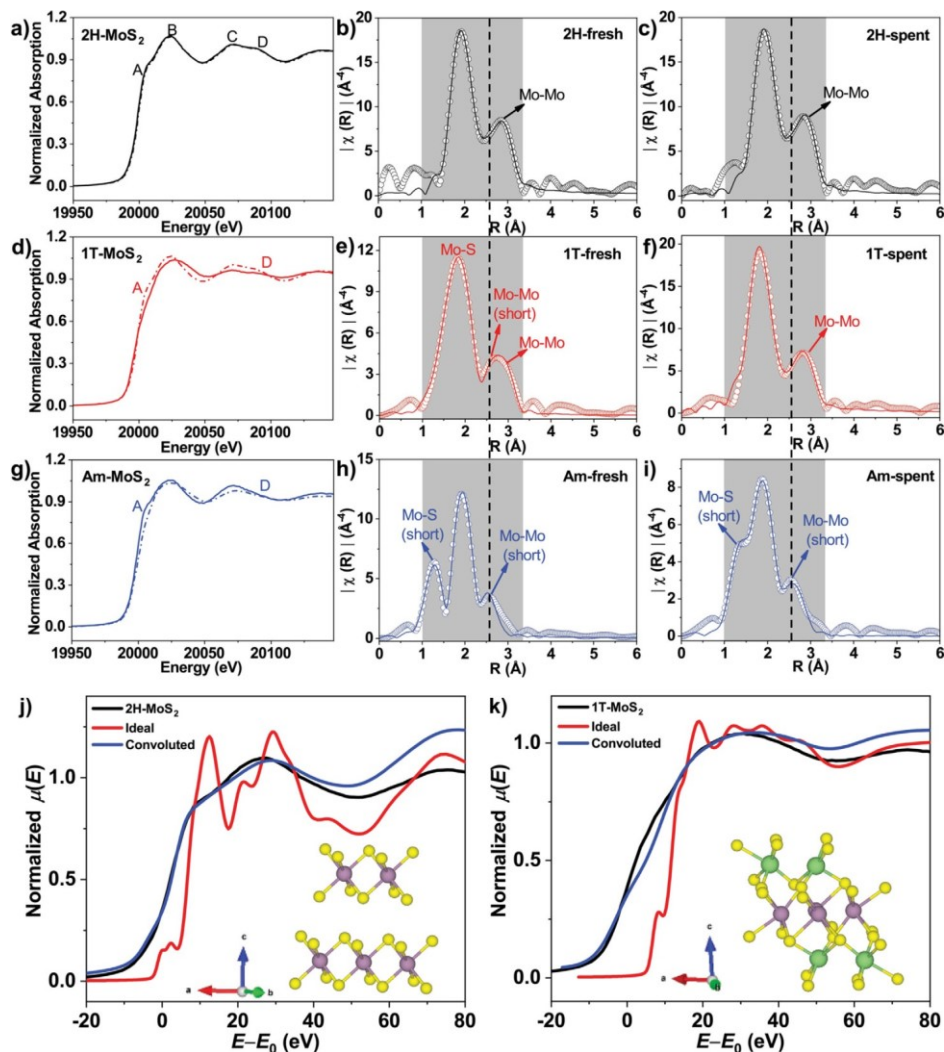


Figure 13. (a,d,g) Mo K-edge XANES spectra of 2H-MoS₂ (a), 1T-MoS₂ (d), and Am-MoS₂ (g) before (solid line) and after (dash line) stability test. b,e,h) Mo Kedge Fourier transform EXAFS (k₃-weighted) of 2H-MoS₂ (b), 1T-MoS₂ (e), and Am-MoS₂ (h) before stability test. c,f,i) Mo K-edge Fourier transform EXAFS (k₃-weighted) of 2H-MoS₂ (c), 1T-MoS₂ (f), and Am-MoS₂ (i) after stability test. j,k) Mo-K edge XANES spectra of experimental data (black curve) and calculated simulation based on hexagonal (j, inset) and monoclinic (k, inset) structure model; red curves represent simulated spectra whereas blue curves represent simulated spectra convoluted with the Mo 1s core-hole lifetime²⁶. (Adapted with permission from ref. 26. Copyright 2019, Wiley-VCH Verlag GmbH & Co. KGaA, Weinheim)

Strategies for MoS₂ engineering to elevate HER performance:

Pristine MoS₂ displayed low catalytic performance for the low concentration of exposed catalytic site. Phase engineering, vacancy engineering, doping, basal plane activation, amorphous, heterojunction or boundary engineering are facile but remarkable strategies for promoting catalytic performance. To meet these demands, exposure edge catalytic sites, make active vacancies, elevate catalytic sites by activate basal plane, modification with cocatalyst were applied. And the relate performance enhancement were compared³⁸. In some cases, the electrocatalyst achieve Pt-like

performance. We make a brief comparison on different strategies on the performance.

Basal plane engineering:

MoS₂'s exposed low-coordinated edge sites are active catalytic site, since the exposed MoS₂ site exhibit moderate hydrogen adsorption behavior that facilitate the water splitting reaction³. As a comparison, pristine basal plane is inert for HER reaction.

To activate the basal plane, single atoms, heterojunctions were applied to introduce alien catalytic site. As depicted in Figure 14 (a-b), Re were introduced into MoS₂ to form alloyed Re_{0.55}Mo_{0.45}S₂ with distort 1T structure. The distort 1T phase was stabilized by Re, and the HER performance were elevated by activated basal plane³⁹. Ruthenium doping and nanocarbon hybridization of MoS₂ have been synthesized by Xing Zhang *et. al.*, and the catalyst shows 50 mV at 10 mA/cm² (overpotential) with 62 mV/dec Tafel value⁴⁰.

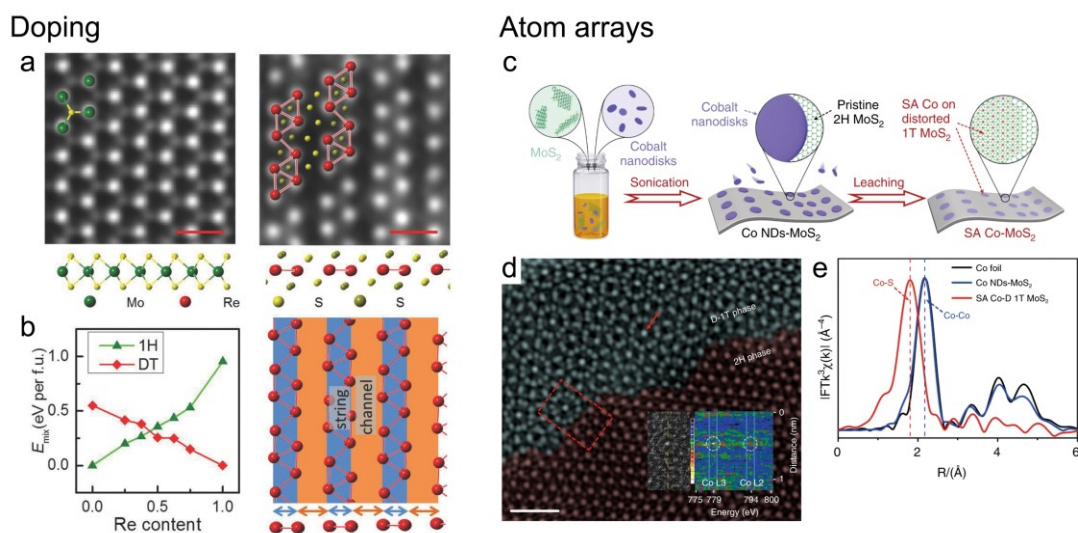


Figure 14. Basal plane activation by doping (a-b) and surface atom array modification (c-e) (a) Structural change diagram represent distort 1T phase induced by Re doping. (b) energy of materials phases relationship with variant Re doping concentration, and the diagram scheme of distort 1T phase with string and channel³⁹. (Adapted with permission from ref. 39. Copyright 2018, Wiley-VCH Verlag GmbH & Co. KGaA, Weinheim) (c) Schematic diagram of the fabrication process for SA Co-D 1T MoS₂. (d) HAADF-STEM HRTEM spectra of 1T-2H heterojunction (e) FT-EXAFS spectra representation of strong interaction between metallic Co atoms and S atoms⁴¹. (Adapted with permission from ref. 41. Copyright 2019, Nature Publishing Group)

And by activating on the basal plane, Pt-like catalytic performance would be introduced⁴¹. As depicted in Figure 14 (c-e), cobalt single atom array modified basal plane were fabricated, since Co atoms on the basal plane act as extra catalytic active site, the catalyst exhibit elevated Pt-like HER performance⁴¹. The Co atom play as the catalytic site, which was identified by using SCN⁻ to poison the Co site. When Co atom were coordinated with SCN⁻ group, the catalysis performance was sharply reduced. Mo single-atom were loaded on monolayer MoS₂'s basal plane, and form

unsaturated Mo atoms⁴². Ni₂P modified on the basal plane of MoS₂ were synthesized by phosphidation of NiMoS₄ to afford Ni₂P/MoS₂. By coupled with conductive N-doped carbon support, Pt-like HER performance were achieved in acidic solution. The HER performance is superior to Pt/C catalyst at high current densities (>200 mA cm⁻²)⁴³. The author attributed the superior catalytic performance to Ni₂P/MoS₂ heterojunction, and the N doped carbon substrate (graphene or CNT) improve the stability and conductivity. Au₂₅ metal cluster were modified on MoS₂ to formulate the interface and display as cocatalyst in HER reaction⁴⁴, the onset potential arrived at -0.2 V vs RHE, the author attribute the enhanced catalytic performance comes from interfacial electronic interaction, and the thiolate (-SR), selenolate (-SePh) ligand on Au clusters show elevating effect to the catalytic performance.

Electrochemical method has been developed to activate the MoS₂⁴⁵. Firstly, atomic layer deposition (ALD) were applied to coat MoS₂ with TiO₂, and form TiO₂ island on MoS₂'s basal plane, and MoO₃ were formed by interaction between MoS₂ and TiO₂. Then TiO₂ were leached by electrochemical activation method, and localized distort MoS₂ basal plane were produced and better HER performance were arrived. The P dopant dramatically reduced Mo valance charge and activate the inert basal plane. O assist P doping into 2H-MoS₂ has been developed and 130 mV onset potential and 49 mV dec⁻¹ Tafel slope were achieved⁴⁶.

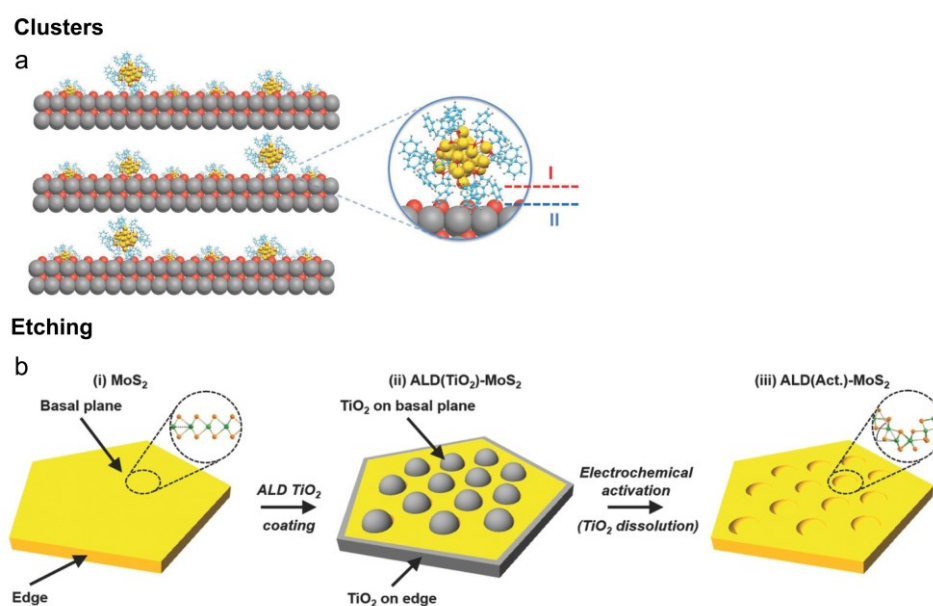


Figure 15. Basal plane cluster modification and etching (a) dual interfacial effect (Interface I and II) in Au₂₅/MoS₂ composite (yellow: Au; red/orange: S; blue: C; gray: Mo)⁴⁴. (b) ALD TiO₂ coating on pristine MoS₂ and the enhancement of the hydrogen evolution reaction activity of ALD(TiO₂) - MoS₂ catalysts via electrochemical activation⁴⁵. (Adapted with permission from ref. 44-45. Copyright 2017, Wiley-VCH Verlag GmbH & Co. KGaA, Weinheim)

Phase engineering by forming 1T phase MoS₂:

MoS₂ compose three mainly different phase, which are 1T, 2H, 3R phases. 2H phase is mostly stable but exhibit with semiconducting performance, the limited conductivity is not friendly to electrocatalysis. It was also report that the 3R phase of MoS₂ depict better HER performance than 2H phase¹⁷. Whereas the metallic 1T phase shows the enhanced water splitting performance.

Hongli Zhu *et. al.* summaries the electrocatalysis performance of 1T metallic phase of MoS₂³². Treated with commercially available stable 2H MoS₂ with n-Butyllithium, large amount batch MoS₂ containing metallic 1T MoS₂ were arrived. However, arrived product by this method only get mixture of metallic 1T MoS₂ and semiconducting 2H MoS₂. Since 1T metallic phase were thermodynamic unstable, it will gradually transfer to stable semiconducting MoS₂ phase⁴⁷. It shows that the extra electron injection into the MoS₂ layer are driving force for the phase conversion. The charge transfer kinetics and H adsorption on the active site were strongly escalated in 1T phase MoS₂ material.

A couple of strategies were applied to stabilize metallic 1T phase. Au-Pd-MoS₂ tri-composite heterointerface were fabricated to induce 1T phase MoS₂ by lattice mismatch effect⁴⁸. Ir-MoS₂ heterointerface were fabricated, based on metal-support interaction by Ir adsorption, 2H phase were partly convert to 1T phase⁴⁹. After performing a modulation calculation, the author discovered that when Ir atoms concentration was large enough, 1T phase were induced. And the author identified that Ir atom and the induced 1T phase were catalytic active site elevate the pristine performance. Wei Ding *et. al.* discovered that 1T phase MoS₂ and WS₂ can be synthesized under high magnetic field, and the resultant 1T-MoS₂ was stable for more than 1 year⁵⁰. The magnetic field could transfer high energy to the material and adjust atomic and molecular alignment, and afford the expected morphology and phase. Gram batch scale synthesis for 1T phase MoS₂ has been developed by Li Song *et. al.*, the synthesis procedure was carried out by hydrothermal reaction between (NH₄)₆Mo₇O₂₄ and thiourea at 200 °C. When NH₄⁺ were introduced into the layer space, the interlayer space was expended to 9 ~ 9.8 Å, and induce formation of distort 1T phase MoS₂ for interaction between NH₄⁺ and MoS₂ layer⁵¹.

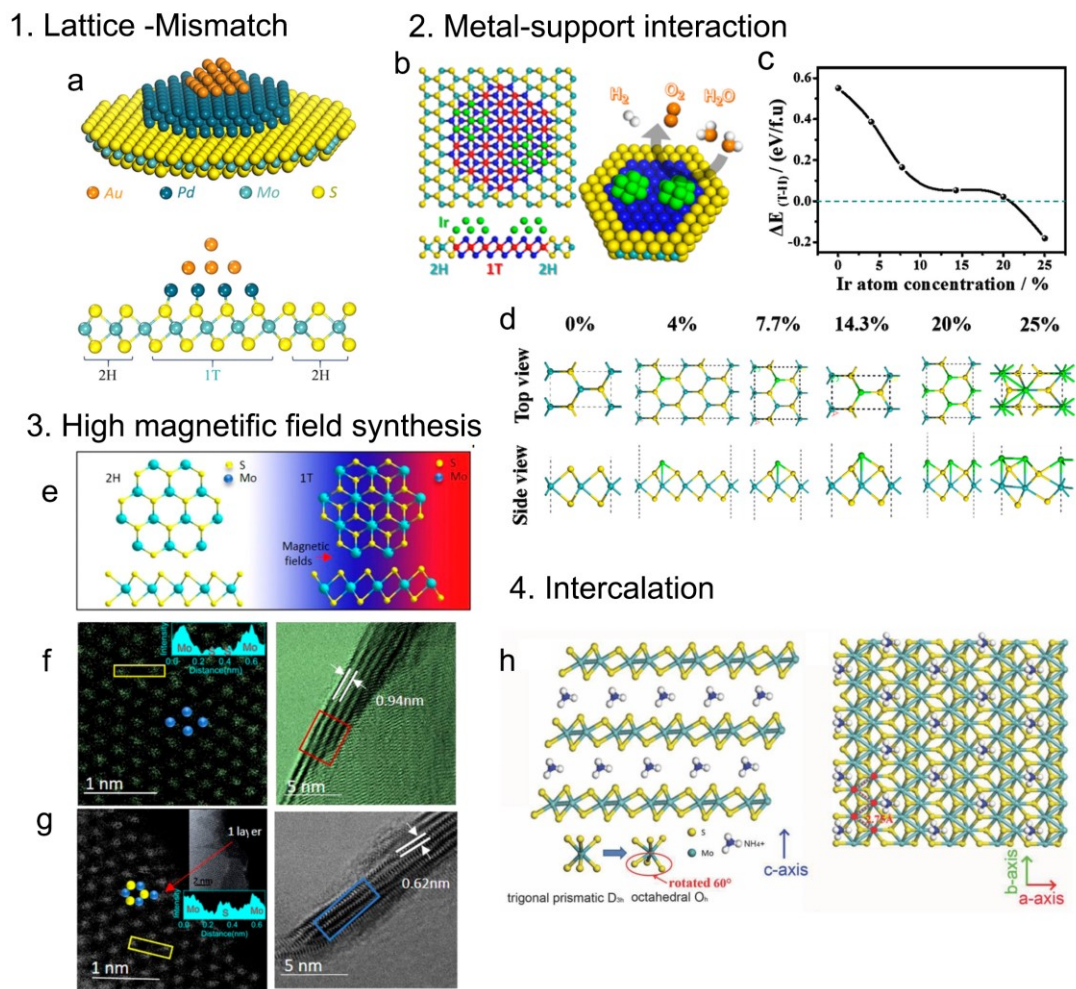


Figure 16. Strategies for fabricate phase convert MoS₂ (a) Lattice-mismatch interface induced phase conversion in Au/Pd-MoS₂⁴⁸ (Adapted with permission from ref 48. Copyright 2019, American Chemical Society.) (b-d) Metal support effect in Ir/MoS₂ induced phase conversion (b) Schematic diagram represents Ir cluster on the basal plane induced phase conversion (c) Energy diagram and (d) Theoretical model between Ir/1T-MoS₂ and Ir/2H-MoS₂ as a function of the atomic concentration of the adsorbed Ir⁴⁹. (Adapted with permission from ref 49. Copyright 2019, American Chemical Society.) (e-g) hydrothermal synthesis of air stable 1T phase under high magnetic field⁵⁰. (Adapted with permission from ref 50. Copyright 2019, American Chemical Society.) (h) interlayer species interaction induced phase conversion. schematic diagram representing of NH₄⁺ intercalated MoS₂ induced distort 1T phase and the corresponding zig-zag chain structure⁵¹. (Adapted with permission from ref. 51. Copyright 2015, Wiley-VCH Verlag GmbH & Co. KGaA, Weinheim)

Doping effect:

Doping atoms can induce phase conversion¹¹. In a Re-MoS₂ material, Re atom substitute MoS₂ shows that phase conversion are much more facile to achieve. Various metal or non-metal atoms were solely or co-introduced into MoS₂ lattice, the introduced atom can modify the electronic

structure of MoS₂ and adjusted the physical properties, induce vacancies, and spontaneously create new catalytic site. In some cases, metal/non-metal co doping introduce superior Pt-like HER performance under high current density. Doping engineering strategies have shown modulate and adjust the physical structure as well as electronic structure of MoS₂, strongly elevate the HER performance.

Metal atoms (Pt, Co, Zn, Ni, W *etc.*) doping effect

Various metal atoms were doped into MoS₂ lattice to elevate the HER performance. According to the theoretical calculation that the dopant can adjust the H adsorption energy to a moderate level and facilitate HER performance⁵²⁻⁵³. It has been found out that the substitute doping of transition metal ions like Re, Tc, Mn stabilized 1T metallic phase for the electron donating effect induced more stabilized 1T electronic structure⁵⁴.

Zn doped MoS₂ was synthesized and the HER performance show that the Zn dopant exhibit superior effect on accelerate the HER reaction (0.13 V overpotential)⁵⁵. The authors attributed the large promotion effect to energy level matching effect as well as morphological effect via thermodynamic and kinetic route. Fe doped MoS₂ were fabricated on Ni foam by simply one-pot solvothermal reaction, and the resultant catalyst display HER performance with a 173 mV overpotential in 0.5 M H₂SO₄ (10 mA cm⁻²), 153 mV in 1 M KOH (10 mA cm⁻²), and also show OER performance with a overpotential at 230 mV (1 M KOH, 20 mA cm⁻²)⁵⁶. Co doped MoS₂ nanosheets bonded on carbon substrate were synthesized and the hybrid catalyst display elevated HER performance⁵⁷. Bao *et. al.* report the single Pt doped few-layer MoS₂, whereas Pt is not working as the catalytic site⁵³.

High valance W metal ions were incorporated into MoS₂ and hybrid with MoO₂ and CNT, the W-MoS₂/MoO₂/CNT exhibit a small Tafel slope of 44 mV dec⁻¹ close to 20 % Pt/C (34 mV dec⁻¹)⁵⁸.

Non-metal atoms (N, P, O, C, Se) doping effect

Non-metal doping like C, O, P, Se were doped into MoS₂, and introduce superior HER performance. N doped MoS₂ were successfully synthesized by Xiao *et. al.*, in their work N atoms were doped on the edge as well as on basal plane, spontaneously boost the catalytic HER performance and exhibit 121 mV (overpotential, 100 mA cm⁻²) and 41 mV dec⁻¹ Tafel slope⁵⁹ (Figure 17). N dopant, PO₄³⁻ intercalated MoS₂ were synthesized by Deng *et. al.*²⁵, the N and PO₄³⁻ induced phase conversion to 1T-MoS₂ (ca. 41 % 2H-MoS₂ were convert), which was higher than that of N doping (ca. 28 %) or PO₄³⁻ intercalation (ca. 10 %). When combined with graphene, the hybrid catalyst emerged 85 mV (overpotential, at 10 mA cm⁻²) and 42 mV dec⁻¹ (Tafel slope).

As depicted in Figure 17, O doped MoS₂ nanosheet were synthesized by hydrothermal reaction between (NH₄)₆Mo₇O₂₄ and extra thiourea. The doped oxygen atom help expend the interlayer space to 9.5 Å, confirmed by XRD as well as HRTEM results⁶⁰. Tapasztó *et. al.* find out that by exposure of MoS₂ monolayer under ambient condition, MoS₂ suffers from a kinetically slow oxygen-substitution reaction to introduce O atoms on the basal plane and can get arrived MoS_{2-x}O_x⁶¹.

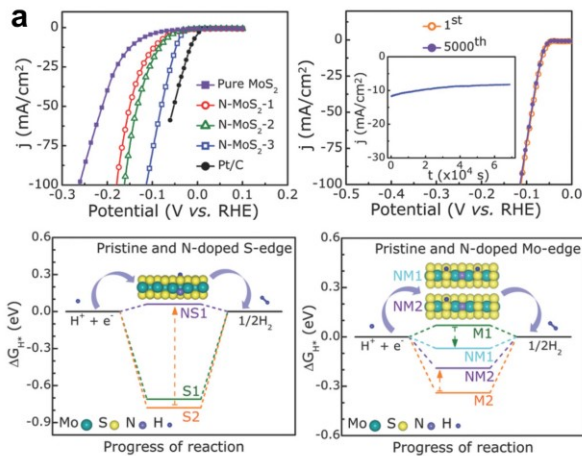
Se were doped into the lattice of MoS₂ to form MoS_{2(1-x)}Se_{2x} with tunable concentration of Se atoms without phase conversion⁶² (Figure 17). The catalyst displayed strong stability without negligible activity loss up to 10000 cycles and the overpotential is small in the range of 80~100 mV.

As depicted in Figure 17, P doped MoS₂ were synthesized by annealing bulk MoS₂ with red phosphorus at 750 °C to form MoS_{2(1-x)}P_x Solid Solution materials⁶³. The best HER performance can be arrived at the constitution of MoS_{0.94}P_{0.53} with an overpotential of 150 mV to reach the current

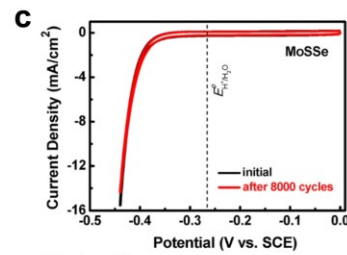
density of 10 mV/cm². P doped MoS₂ (with interlayer distance of ~9.0 Å) were also synthesized by Liu *et. al.* and the HER performance exhibit ~43 mV (overpotential, 10 mA/cm²) and 34 mV/dec (Tafel slope) as well as long-term catalytic stability⁶⁴.

Zang *et. al.* synthesized C doped MoS₂ by controlled sulfurization of Mo₂C, and the prepared MoS₂ displayed an unprecedented overpotential of 45 mV at 10 mV/cm² in the alkaline environment, which is just a bit lower than commercial Pt/C⁶⁵ (Figure 17). The electronic as well as coordination structure were significantly changed by incorporation of carbon atoms, the authors attribute the elevated HER performance to the orbital modulation, that C induced empty 2p orbitals perpendicular to MoS₂'s basal plane, facilitate water adsorption and dissociation.

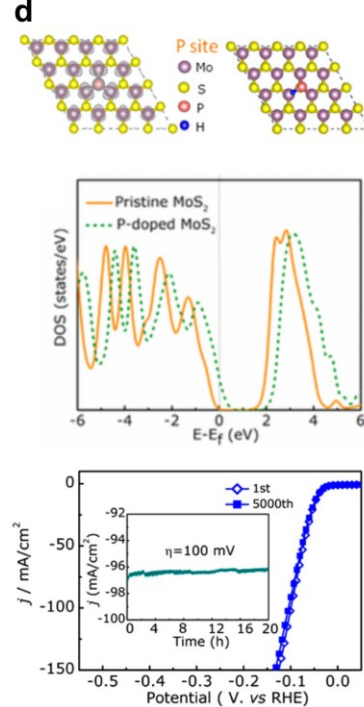
N doping



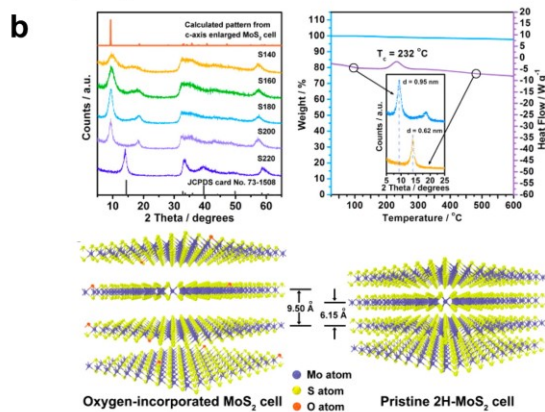
Se doping



P doping



O doping



C doping

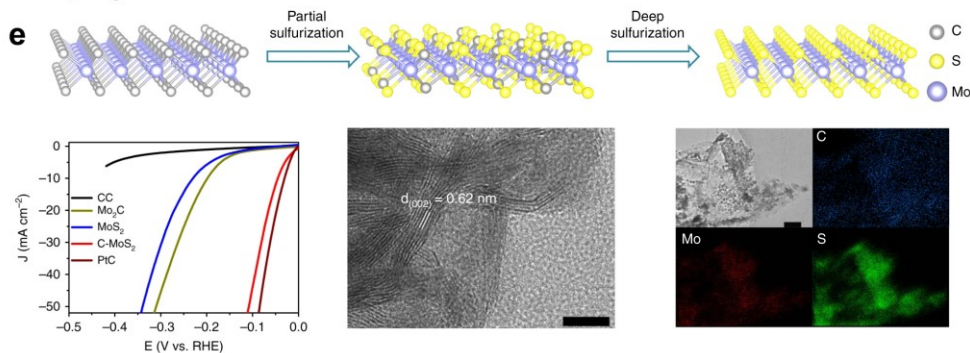


Figure 17. Non-metal atoms (N, P, O, C, Se) doping effect of MoS₂ towards elevated HER performance. (a) N doping. The schematic illustration of the synthesis of C-MoS₂ and MoS₂.⁵⁹ (Adapted with permission from ref. 59. Copyright 2017, Wiley-VCH Verlag GmbH & Co. KGaA, Weinheim) (b) O doping. The XRD patterns of O incorporated MoS₂ and the structure diagram scheme.⁶⁰ (Adapted with permission from ref 60. Copyright 2019, American Chemical Society.) (c) Se doping. CV curves of MoSSe before and after 8000 potential cycles⁶² (Adapted with permission from ref. 62. Copyright 2015, American Chemical Society.) (d) P doping. CV curves of

P doped MoS₂ before and after 5000 potential cycles⁶⁴ (Adapted with permission from ref. 64. Copyright 2017, American Chemical Society.) (e) C doping. The schematic diagram of synthesis of C doped MoC⁶⁵. (Adapted with permission from ref. 65. Copyright 2019, Nature Publishing Group)

Co-doping effect:

Co-doping method exhibit dual activation ability by activation on different catalytic site. Co-doping strategies were employed by D. Deng *et al.*, doping with Se on the basal plane surface and Co in the inner layer, the HER performance exhibit with a overpotential of 132 mV at 10 mA cm⁻². The author consider that the inner-layer Co-doping and the surface Se-doping exhibit a synergic effect to improve the HER performance, attributing to the enriched catalytic site and hydrogen adsorption optimizing. And in current density at 1000 mA cm⁻², the Co, Se co-doped MoS₂ overpotential reach 382 mV, much lower than commercial 40 % Pt/C, and working continuously for at least 360 h without any decay. Huang *et al.* found that Ni, O co-doped 1T phase MoS₂ catalyst exhibit Pt-like hydrogen evolution performance in alkaline solution⁶⁷. In which Ni, O were synergistic doped in 1T MoS₂, and the overpotential at lower current density (< 80 mA cm⁻²) exhibit better performance than commercial 20 % Pt/C. Xiong *et al.* discovered cobalt doped MoS₂ show good HER performance under acidic as well alkaline solution⁶⁸.

Mn, N co-doped MoS₂ was synthesized by Su *et al.*, the electronic structure of the doped MoS₂ material exhibit strongly enhanced HER performance with the overpotentials of 66 and 70 mV at 10 mA cm⁻² in alkaline and phosphate-buffered saline media, respectively⁶⁹. O, P co-doped MoS₂ was synthesized by Dongdong Zhu *et al.* via hydrothermal treating of MoS₂ with NaH₂PO₂, and the experimental results show that the co-doped MoS₂ display better HER performance than O doped MoS₂⁷⁰. P, Se co-doped MoS₂ were fabricated using C₄H₁₄N₃PS and Na₂SeO₃ as additive, the resultant P, Se co-doped MoS₂ display better performance than mono-doped MoS₂⁷¹. F, N co-doped MoS₂ were synthesized to activate basal plane and onset overpotential of 110 mV and 57 mV dec⁻¹ Tafel slope were achieved⁷².

Vacancy engineering:

Vacancies are typical catalytic site that not limited to HER reaction⁷³. Mo vacancies and S vacancies were fabricated in MoS₂ to elevate the catalytic HER performance. Sulfur vacancy can be introduced by electrochemical reduction⁷⁴, etch by H₂⁷⁵, H₂O vapor⁷⁶.

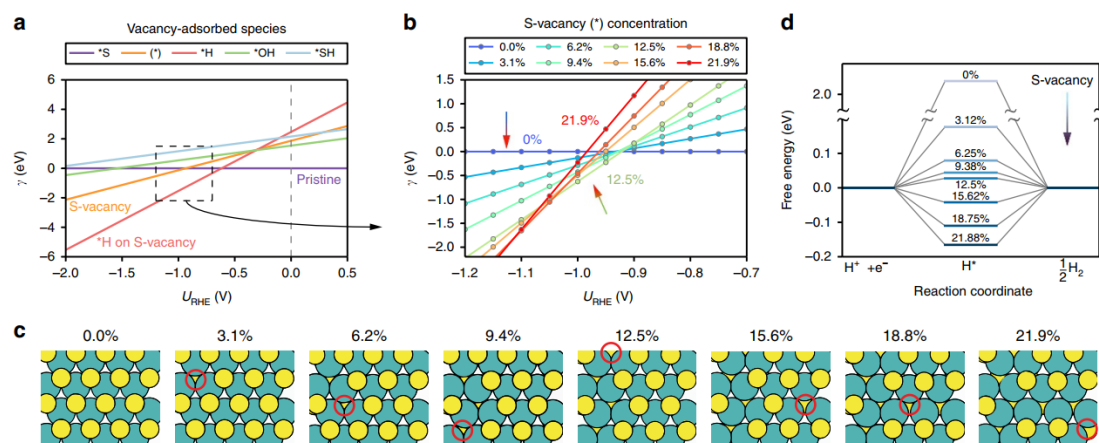


Figure 18. (a) Surface energy per unit cell for 2H-MoS₂ as a function of applied potential for the basal plane of 2H-MoS₂ with different adsorbate species at a fixed sulfur vacancy (3.1%). (b) Surface energy per unit cell for a range of S-vacancy concentrations, without any adsorbates. The concentration of S-vacancies varies from 0 to 21.9% within the narrow range of 1.0 V to 1.1 V. (c) When the S-vacancy sites are generated in succession, S-vacancies are most stable when formed next to an existing S-vacancy. (d) Free energy diagram for the HER on S-vacancy sites⁷⁴. (Adapted with permission from ref. 74. Copyright 2017, Nature Publishing Group)

As depicted in Figure 18, Charlie Tsai *et al.* applied the electrochemical strategies to introduce sulfur vacancies into MoS₂ materials, and the HER performance were examined⁷⁴. By applying different potential, the extent of desulfurization was varied, and HER performance were spontaneous alternated.

Sulfur vacancy were fabricated by William A. Goddard III *et al.*, they made a detailed study on the HER reaction on the sulfur vacancies. They discovered that the sulfur vacancies are favored to elevate the HER performance for that the transition state energy is closer to the product, and it can get a more moderate Tafel slope⁷⁷. Cao *et al.* synthesized the MoS₂ materials and introduced variant amount of sulfur vacancies by simply calcinate molybdenum chloride (MoCl₃) with sulfur under 850 °C, they find that the 7~10 % sulfur vacancies density and better crystallinity help entrance towards better HER performance⁷⁸.

As depicted in Figure 19, Xin Wang *et al.* introduced homogeneously distributed sulfur vacancies by H₂O₂ etching method, by systematically adjusting of etching time, temperature, and H₂O₂ concentration, various S-vacancy state can be achieved⁷⁹. This systemic study shows a better understanding between the structure, concentration of sulfur vacancy and the relate HER performance. D. Voiry *et al.* made a systematic study on the variant amount sulfur vacancies relation with the HER performance. They clarified that when point S vacancy were introduced to MoS₂ rapid elevating of HER performance can be tracked, while more S atoms were removed (atom ratio: S/Mo > 1.7), the catalyst is dominated by the uncoordinated Mo site and S vacant⁸⁰. Sulfur vacancies concentration were introduced by regulating reduction conditions (atmosphere and temperature).

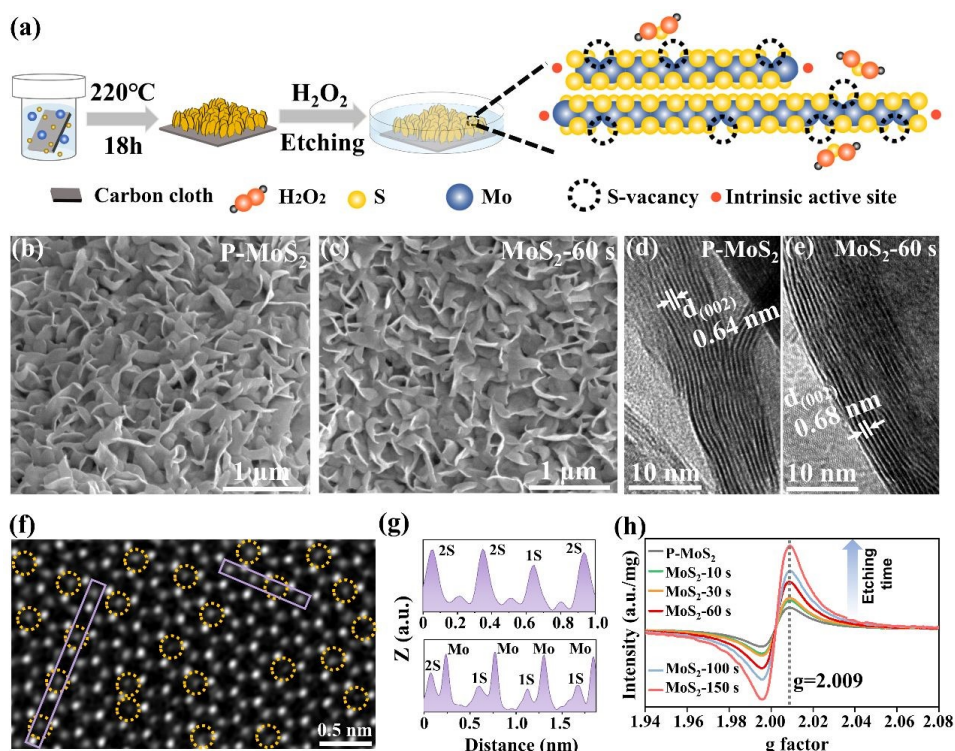


Figure 19. (a) Schematic of the chemical etching process to introduce single S-vacancies. b-e) SEM and HRTEM images of (b, d) P-MoS₂ and (c, e) MoS₂. f-g) The STEM image together with the line profiles extracted from the areas marked with purple rectangles of a CVD-grown monolayer MoS₂ flake film after etching. The yellow dotted circles represent the S-vacancies. h) EPR spectra of etched MoS₂ with different etching durations⁷⁹. (Adapted with permission from ref. 79. Copyright 2020, American Chemical Society.)

As depicted in Figure 20, pristine 2H MoS₂ were annealed in Zn vapor to forming sulfur vacancies and Zn atom dopant. The results shows that the Zn can induce sulfur vacancies and Zn dopant can also active the adjacent S vacancy site, and elevate HER performance⁸¹. By reduction reaction with Zn, MoS₂ were cracked into small pieces (pristine 100~200 nm sheet were cracked into sub-25 nm sheet).

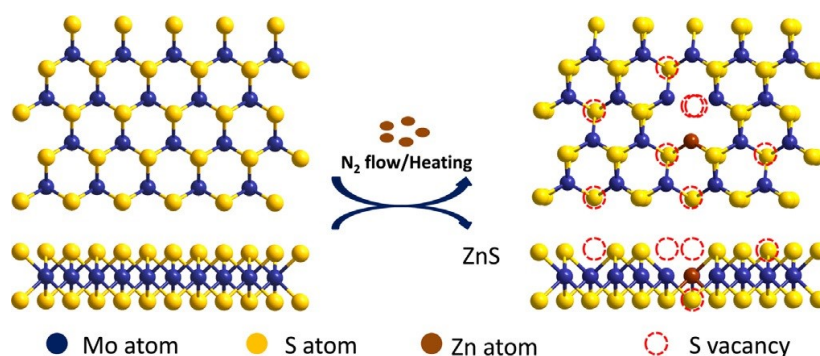


Figure 20. Diagram of the experimental creation of S vacancies in a 2H-MoS₂ nanosheet by Zn vapor annealing⁸¹ (Adapted with permission from ref. 81. Copyright 2019, Wiley-VCH Verlag GmbH & Co. KGaA, Weinheim).

Strained sulphur vacancies were introduced into MoS₂ material and HER performance were discovered, it was found that the performance was elevated by carried out the HER reaction under different sulphur concentration (0~21.9 %), and the best catalytic performance is not followed with higher concentration of vacancies. The theoretical results show that the hydrogen adsorption energy can be modified by adjust the strain on S vacancy, and elevate HER catalytic reaction⁸².

16 types of different structural defects including point defects, grain boundaries were analyzed by first-principle calculations to clarify how the intrinsic vacancies influence the MoS₂'s HER performance⁸³. And using amendatory band-center model to examine different HER performance along various kinds of vacancies.

Interlayer space expending and intercalation:

Edge-site low coordinated atoms were regard as the best catalytic site, since interlayer engineering can induce the local chemical environment and electronic structure changes, the relate catalytic performance were modulated.

Intercalation of Li⁺ into MoS₂ layer space is widely applied for MoS₂ exfoliation. What's more, chemical intercalation is a traditional and welcomed strategy for metallic MoS₂. G Eda. *et. al.* used *n*-Butyllithium compound to exfoliate MoS₂ in hexane under Ar atmosphere²². Polymers, molecule, cationic species, organometallic species has been intercalated into the layer of MoS₂ to expend the layer distance⁸⁴⁻⁸⁶.

The expend layer can reduce the resistance during the ion in the layer space. By intercalate by poly(ethylene oxide), the interlayer distance is expanded to 1.45 nm⁸⁷. Hydrothermal reaction using (NH₄)₆Mo₇O₂₄·4H₂O with thiourea as reactant would yield MoS₂ with a 0.95 nm interlayer space⁶⁰. The relative study shown that NH₄⁺ were intercalated into the layer space⁵¹.

Increasing interlayer distance would impact the band energy of MoS₂ and electronic structure. As depicted in Figure 21, Sun *et. al.* synthesized the enlarged MoS₂ with an interlayer distance of 9.4 Å, in this way the stacked MoS₂ with enlarged interlayer's perform like the freestanding monolayer MoS₂. Theoretical results shown that the expended layer distance induce the band gap shift upwards along the Fermi Level by ~0.1 eV (Figure 21b), and enlarged layer distance facilitate the H adsorption on MoS₂'s edge site^{38, 86}.

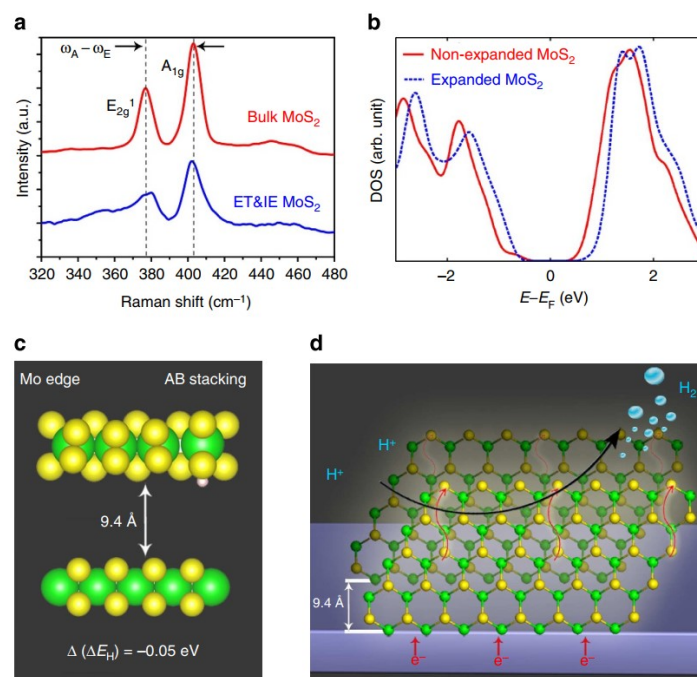


Figure 21. (a) Raman spectra (b) The projected DOS of bulk MoS₂ and ET&IE (edge-terminated and interlayer-expanded) MoS₂. (c) DFT calculation of the change in hydrogen adsorption energy. (d) Schematic representation of the edge-terminated MoS₂ on glassy carbon electrode for HER³⁸. (Adapted with permission from ref. 38. Copyright 2015, Nature Publishing Group)

Ultrathin MoS₂ with a 9.5 Å interlayer distance coupled to N-doped reduced graphene oxide was synthesized by a one-step hydrothermal reaction⁸⁸. As depicted in Figure 22, the 9.5 Å larger interlayer present a preferable ΔG_{H^*} value of -0.052 eV, while the pristine MoS₂ with 6.3 Å shows -0.201 eV. The enlarged layer distance display better proton/electron adsorption and hydrogen release step, and superior HER performance was verified.

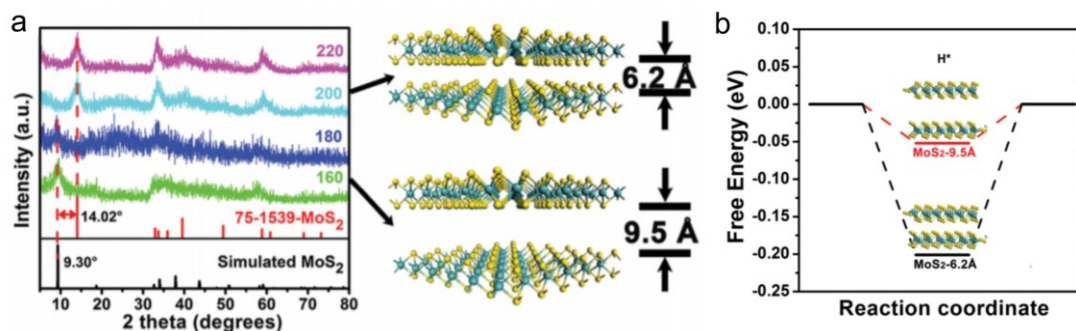


Figure 22. (a) XRD patterns of MoS₂/N-RGO-T nanocomposite prepared at different temperatures from 160 to 220 °C. At the right, structural models of MoS₂ with the interlayer spacing of 6.2 and 9.5 Å, respectively. (b) Calculated free energy diagram for HER on MoS₂-6.2 Å and MoS₂-9.5 Å⁸⁸. (Adapted with permission from ref. 88. Copyright 2016, Wiley-VCH Verlag GmbH & Co. KGaA, Weinheim)

Edge exposure engineering:

Edge sites are catalytic active site for the HER reaction, exposure of large amount of edge site are fundamental strategies for achieve high-performance HER catalysts. Self-assembly, novel synthesis method like chemical vapor deposition (CVD)⁸⁹⁻⁹⁰, surfactant-assist low-temperature solution process, hierarchical nanostructure fabrication strategies were applied to exposure with more active edge site. As depicted in Figure 23, Cui *et. al.* deposit 5 nm Mo layer on quartz, SiO₂/Si substrate and then Mo react with S vapor to afford vertically aligned MoS₂⁹⁰. Decreasing of the Tafel slope to 49 % can be achieved by selective steam etching method by expose with more active edge site^{76, 91-92}. As depicted in Figure 24, by adjusting precursor composition, Ruitao Lv *et. al.* using electrospinning strategies fabricate carbon nanofibers with large amount of exposed MoS₂ edge site⁹¹.

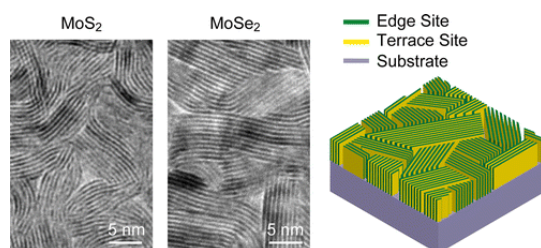


Figure 23. (left) TEM image of a MoS₂, MoSe₂ films with edge-terminated structures. (right) Idealized structure of edge-terminated molybdenum chalcogenide films with the layers aligned perpendicular to the substrate⁹⁰ (Adapted with permission from ref. 90. Copyright 2013, American Chemical Society.)

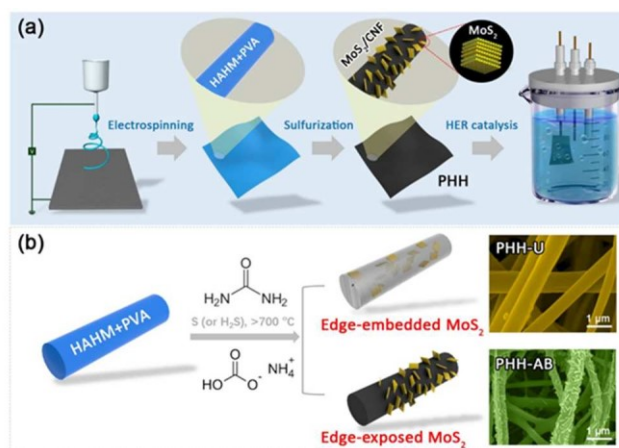


Figure 24. (a) Schematic illustration of electrospinning synthesis of MoS₂/CNF nanocomposite and HER catalysis. (b) Controlled growth of MoS₂ nanoplates in the CNFs from different precursors, and the corresponding structures with MoS₂ nanoplates embedded inside (the top right SEM image) or exposed outside (the bottom right SEM image) of CNFs⁹¹. (Adapted with permission from ref. 91. Copyright 2018, American Chemical Society.)

Edge site catalytic activity can be further controlled by assembly on the support. Nørskov *et. al.* discovered that the support can induce significant changes in the hydrogen binding energy by long-range van der Waals (vdW) forces, and the HER performance were elevated⁹³. Experimental result also show the strong elevated HER performance by metal support, Cao *et. al.* found that the interfacial interaction with the metal substrate can elevate hydrogen evolution performance⁹⁴.

Amorphous MoS₂:

Amorphous MoS₂ has been found to show enhanced catalytic performance than pristine MoS₂⁹⁵, for that in amorphous MoS₂, the Mo-Mo bond is much shorter and is pivotal to elevated HER performance²⁶. Amorphous MoS₃ were fabricated by Jaramillo *et. al.* by wet chemical synthesis procedure, and during the electrocatalytic test, surface MoS₃ were transferred to amorphous MoS₂ to exhibit catalytic performance ~ 200 mV (10 mA cm^{-2})⁹⁶. Sang Chul Lee *et. al.* synthesis amorphous MoS₂ and explored the electrochemical HER performance with the TEM characterization⁹⁷. They discovered that the amorphous MoS₂ can crystallize and deactivated during HER. As depicted in Figure 25, Phong D. Tran *et. al.* clarified the detailed catalytic route of amorphous MoS₂ by [Mo₃S₁₃]²⁻ polymer contain four types of distinct potential catalytic site, and verified that molybdenum hydride moieties was responsible for the active HER catalytic site⁹⁸.

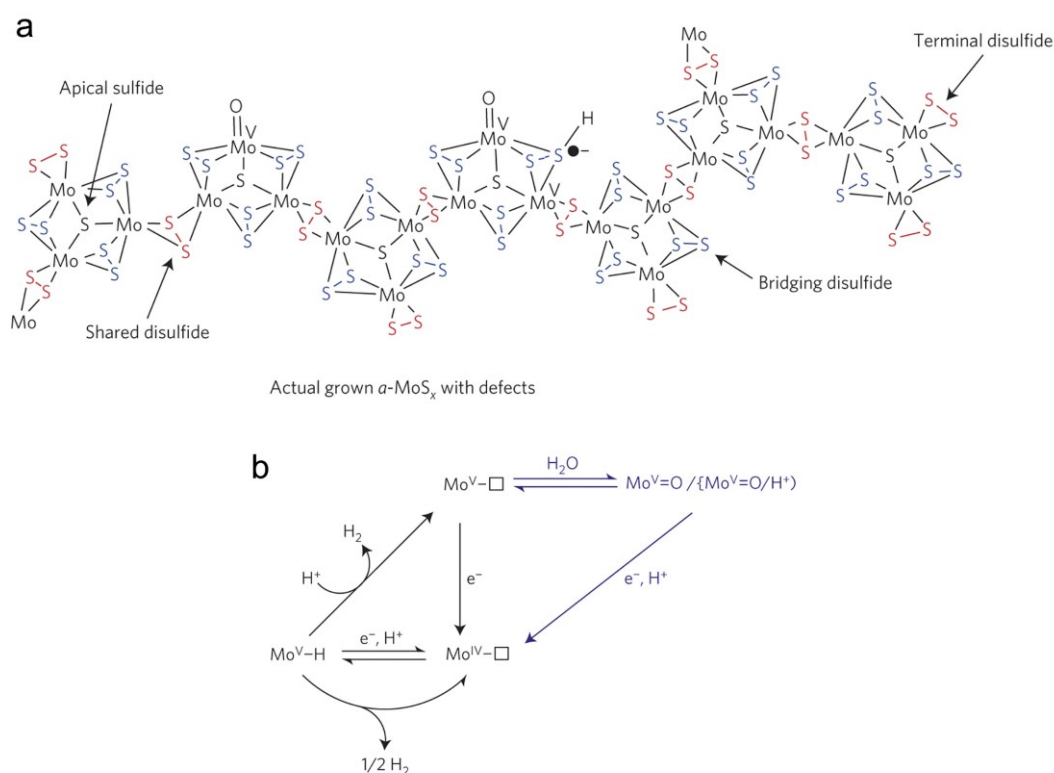


Figure 25. (a) Schematic structural for amorphous MoS₂ four different ligands: apical sulfide μ -S²⁻, bridging disulfides (S-S)_{br}²⁻, shared (S-S)_{sh}²⁻ and terminal disulfides (S-S)_t²⁻ (b) Proposed catalytic pathway for H₂ evolution⁹⁸. (Adapted with permission from ref. 98. Copyright 2016, Nature Publishing Group)

Heterojunction:

The heterojunction can elevate the HER performance since the favored chemisorption behavior⁹⁹, modification of the electronic states.

MoS₂ boundary of hetero 1T-2H phase were constructed, and the heterojunction display superior HER performance in both acidic and alkaline solution as well as long-term stability⁹⁹. In their work,

J. Zhu *et al.* made a detailed comparison of catalytic performance between 2H-2H domain and 2H-1T domain, and the theoretical results show that the 2H-1T boundary exhibit $\Delta G_{H^*} = -0.13$ eV (close to Pt (111) surface as well as Mo-edge of 2H-MoS₂). Long term test show that the boundary catalyst is stable. In-plane MoS₂ heterojunction has also been synthesized by Zili Wu *et al.*, and find the similar results¹⁰⁰.

MoS₂ hybrid materials have been synthesized by forming heterojunction with carbon species, graphene, metal oxide, metal hydroxide, nitride, to elevate catalytic performance by synergistic effect.

MoS₂@TiO₂ heterojunction hybrid material has been synthesized and the hybrid materials owns better performance based on promoting the carrier transfer efficiency and prevent MoS₂'s aggregation¹⁰¹. MoS₂/CoS₂ were fabricated by sulfur assist pyrolysis of Co/Mo-MOF with 4~7 nm thick nanosheet, and the HER overpotential was 75 mV (10 mA cm⁻², 1 M KOH; commercial Pt/C's overpotential: 60 mV), which was much lower that MoS₂ (309 mV) or CoS₂ (525 mV)¹⁰². And MoS₂/CoS₂ shows an overpotential around 99 mV (10 mA cm⁻², 0.5 M H₂SO₄), 151 mV (10 mA cm⁻², 0.5 M Na₂SO₄). MoS₂-Ni₂O₃H were synthesized by two sequence hydrothermal reaction, the resultant hybrid catalyst show a overpotential of 84 mV at 10 mA cm⁻², 217 mV at 200 mA cm⁻² (1 M KOH)¹⁰³. Ni(OH)₂/MoS₂ hybrid materials has been developed and display superior activity than Pt/C in alkaline HER¹⁰⁴. The hybrid catalyst were formed by quantum 1T-MoS₂ decorated with Ni(OH)₂, exhibit overpotential of 57 mV (10 mA cm⁻²) and 112 mV (100 mA cm⁻²) in 1 M KOH. The intensified HER performance in alkaline can be attribute from Ni(OH)₂ that provide hydroxyl adsorption active sites, which facilitate the HER process. As depict in Figure 26, MoS₂ were firstly fabricated on carbon cloth, then Ni(OH)₂ nanoparticles were loaded on MoS₂ by electrodeposition¹⁰⁵. Based on the synergistic interface effect of Ni(OH)₂/MoS₂, the HER performance were significantly elevated.

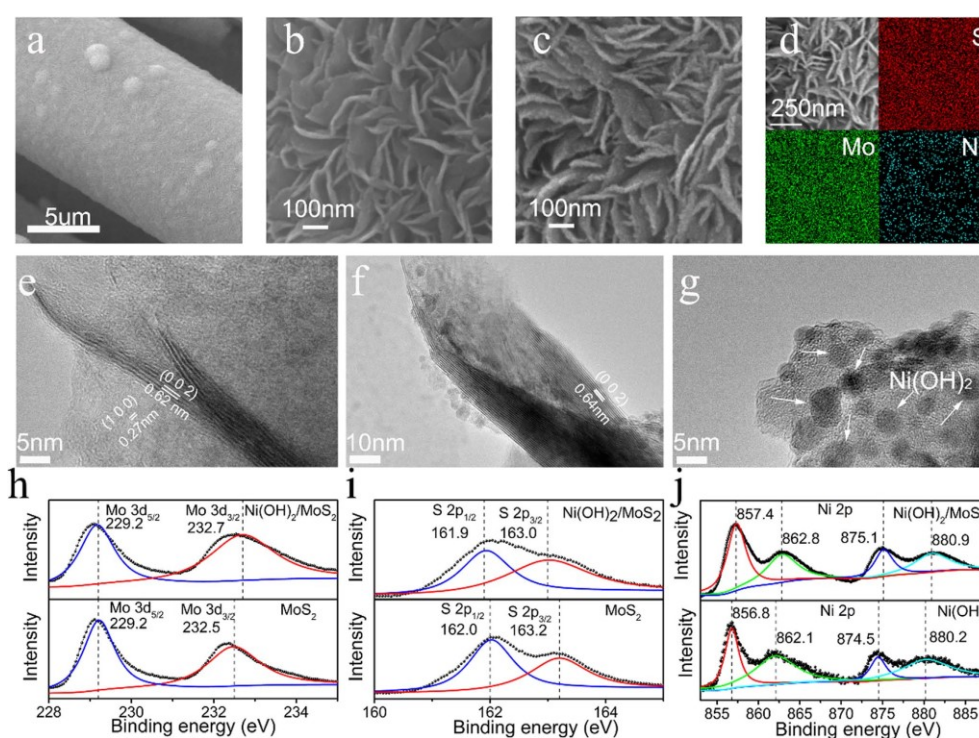


Figure 26. (a-b) SEM images of MoS₂@CC with different magnifications. (c-d) SEM images and EDX mappings of Ni(OH)₂/MoS₂@CC. (e) TEM image of MoS₂@CC. (f-g) TEM image of Ni(OH)₂/MoS₂@CC. (h-j) XPS spectra of Mo 3d, S 2p and Ni 2p¹⁰⁵. (Adapted with permission from ref. 105. Copyright 2017, Elsevier Ltd.)

Yuting Luo *et al.* discovered Co(OH)₂ confined MoS₂ shows elevated HER performance in alkaline solution exhibiting with 15 mV overpotential¹⁰⁶ The hybrid materials are synthesized by two-step strategies. In the first step, Li⁺ were introduced into the layer space of MoS₂ by the typical Butyllithium treatment method. Then in the second step, Co²⁺ were exchanged into alkaline media to formulate MoS₂ intercalated with Co(OH)₂ nanoparticles. Yang *et al.* fabricate 2H-MoS₂ and NiCo-LDH hybrid materials that exhibit a overpotential at 78 mV (10 mA cm⁻², 1 M KOH)¹⁰⁷.

As depicted in Figure 27, MoS₂/CoSe₂ hybrid catalyst were synthesized by Ming-Rui Gao *et al.*, the hybrid material shows intensified HER performance¹⁰⁸. The synthesis procedure was carried out with two steps. Firstly, CoSe were synthesized and stabilized with EDTA. Then the as-synthesized CoSe nanobelt were mixed with (NH₄)₂MoS₄ and undergo hydrothermal reaction to get the MoS₂/CoSe₂ hybrid catalyst. And the electrocatalysis performance is elevated when the catalyst undergoes the HER reaction.

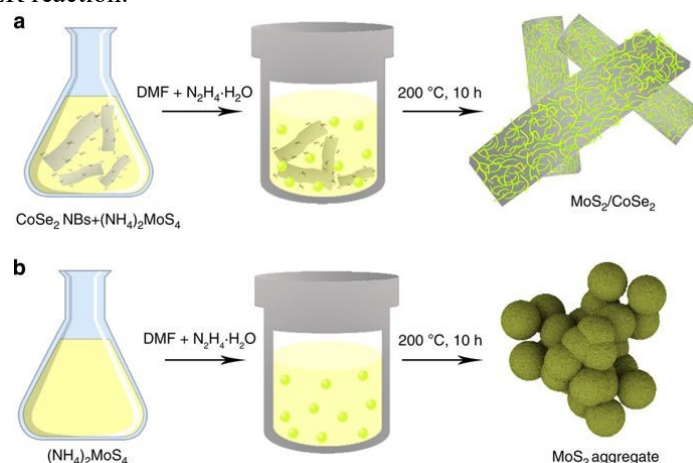


Figure 27. (a) Solvothermal synthesis with CoSe₂/DETA nanobelts as substrates for preparation of MoS₂/CoSe₂ hybrid. (b) Solvothermal synthesis without CoSe₂/DETA nanobelts leads to free MoS₂ nanosheet aggregates¹⁰⁸. (Adapted with permission from ref. 108. Copyright 2015, Nature Publishing Group)

MoS₂ has also been loaded on Ti₃C₂ applying microwave heating with (NH₄)₂MoS₄ as precursor molecules. The author see that the MoS₂ is vertically aligned on Ti₃C₂ and edge active catalytic site is totally exposed¹⁰⁹. Thin MoS₂ nanosheet (4~6 layers) were loaded on TiN nanorods, and the resultant hybrid catalyst exhibit a low overpotential of 119 mV (10 mA cm⁻²), 44.8 (Tafel slope), and long term stability¹¹⁰. MoS₂-MoP heterojunction materials has been synthesized by Aiping Wu A *et al.* by two-step synthesis procedure¹¹¹. Firstly, hierarchical MoS₂ were synthesized and then as-synthesized MoS₂ were react with NaH₂PO₂ to get MoP coated MoS₂. The achieved hierarchical MoS₂@MoP core-shell catalyst HER performance exhibit overpotential of 42 mV (10 mVcm⁻² in 1M KOH), 29 mV (10 mV cm⁻² in 0.5M H₂SO₄). Cu₇S₄@MoS₂ hetero-nanocomposite show the HER performance with a 206 mV overpotential (0.5 M H₂SO₄, 200 mA cm⁻²)¹¹². And after CV activation for 11000 cycles with a Pt wire counter electrode, the catalytic performance is better than 20 % commercial Pt/C catalyst (overpotential: 26 mV in 10 mA cm⁻²). The characterization show that during the CV activation, Pt atoms on Pt wire were dissolved but deposit on Cu₇S₄@MoS₂.

Nano structural and Substrates engineering:

Electrochemical process can be elevated by mass transport, electron transportation and diffusion, avoid of restacking, *etc*¹¹³. Constructing of various nanostructures are simply but efficient procedures for elevate the electrochemical performance¹¹⁴. Various structures like hierarchical structure¹¹⁵, quantum dot¹¹⁶, porous¹¹⁷, hollow sphere¹¹⁸, loading on substrate^{94, 119} were applied. As depicted in Figure 28 (a-b), assembling MoS₂ nanosheets into three-dimensional (3D) superstructure has been developed to access to maximum reactants and expose with more active site, high level electrochemical performance were achieved¹¹⁵. As depicted in Figure 28 (c), MoS₂ quantum dot (3.6 nm) were synthesized by one-step hydrothermal reaction and display with 160 mV overpotential with a 59 mV dec⁻¹ Tafel slope¹¹⁶. As depicted in Figure 28 (d), mesoporous MoS₂ with a double-gyroid (DG) morphology were synthesized by Thomas F. Jaramillo group, which preferentially expose abundant active edge sites on a large-area thin film, the mesoporous MoS₂ were formed by etching of the silica template¹¹⁷. As depicted in Figure 28 (e), hollow spheres were fabricated and elevated HER performance were achieved with a 112 mV onset overpotential ($\eta=214$ mV at 10 mA cm⁻²)¹¹⁸. hydrothermal reaction between sodium molybdate, thioacetamide and oxalic acid at 200 °C for 24 h, and then calcite at 800 °C in Ar atmosphere to form hollow structure and crystallization. As depicted in Figure 28 (f), MoS₂ were fabricated onto the carbon cloth vertically, which improve electron delivery effectively, and the HER performance were significantly elevated ($\eta=205$ mV at 200 mA cm⁻²)¹¹⁹. As depicted in Figure 28 (g), MoS₂ were coupled to Ti substrate and forming interfacial tunneling barrier between Ti and MoS₂, which elevate HER performance that superior than Pt⁹⁴.

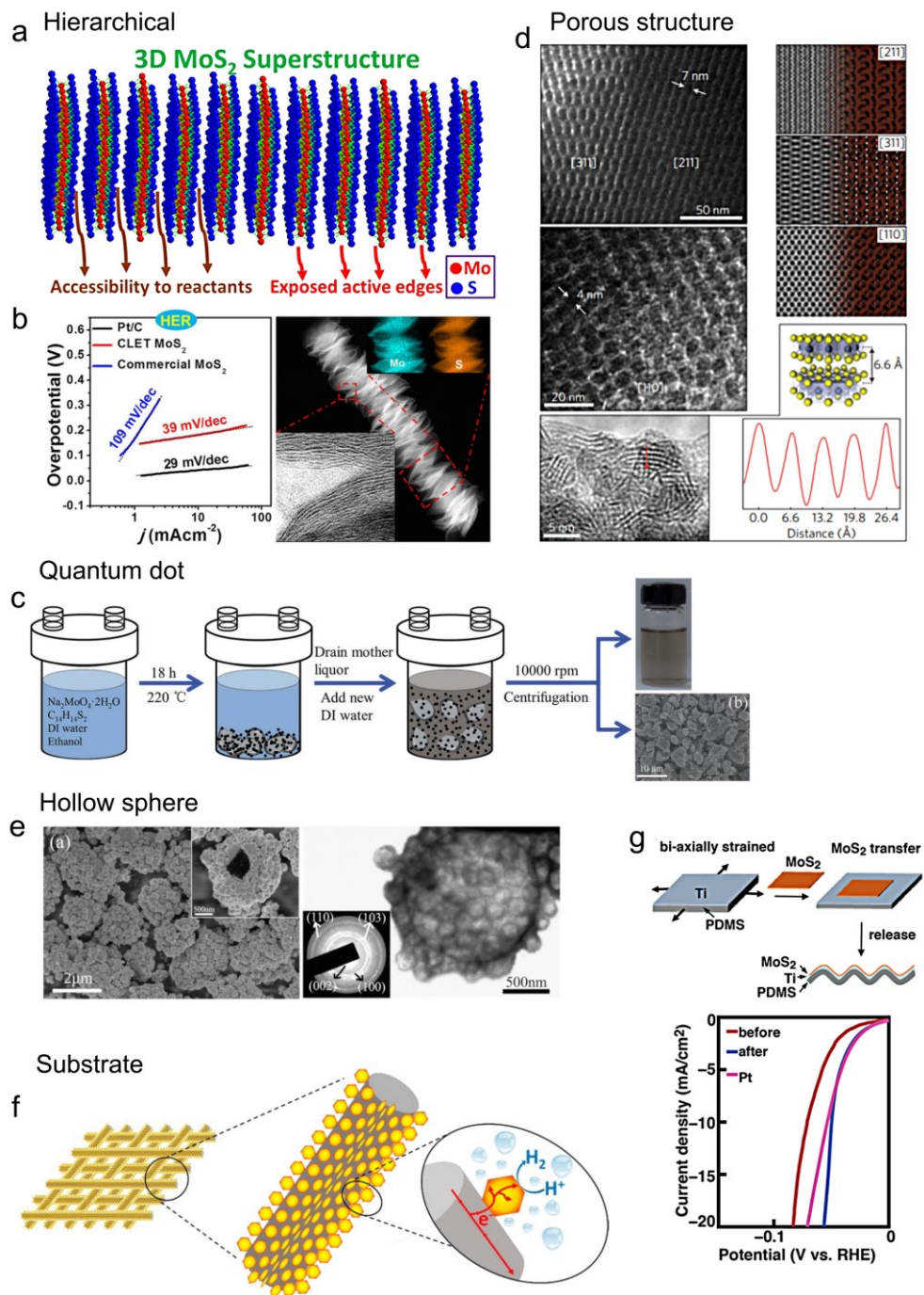


Figure 28. Nano structure and substrate fabrication of MoS₂ (a-b) Hierarchical structure of MoS₂ (a) diagram and (b) HER performance, TEM photo of 3D MoS₂ Superstructure with Maximized Accessibility to Reactants and Exposed Active Edges¹¹⁵ (Adapted with permission from ref. 115. Copyright 2016, American Chemical Society.) (c) MoS₂ quantum dot. synthesis procedure to prepare MoS₂ QDs by using a hydrothermal approach¹¹⁶ (Adapted with permission from ref. 116. Copyright 2016, American Chemical Society.) (d) porous MoS₂. Engineering the surface structure of MoS₂ to preferentially expose active edge sites for electrocatalysis¹¹⁷. (Adapted with permission from ref. 117. Copyright 2012, Nature Publishing Group) (e) MoS₂ hollow sphere. SEM and TEM spectra of micro-nano multi-hollow MoS₂¹¹⁸ (Adapted with permission from ref. 118. Copyright 2016, American Chemical Society.) (f) Schematic diagram for synthesis of MoS₂ ⊥ carbon cloth

substrate to expose as many MoS₂ edge sites¹¹⁹ (Adapted with permission from ref. 119. Copyright 2015, American Chemical Society.) (g) Schematic illustration for the process of crumpling MoS₂ films and LSV curves shows better performance than Pt⁹⁴ (Adapted with permission from ref. 94. Copyright 2020, American Chemical Society.)

MoS₂'s layer is also correlated to the HER performance. MoS₂ with 1~4 layers were synthesized and the catalytic performance towards MoS₂ layer number were studied, it shows that the catalytic performance is consistent with the layer number¹²⁰.

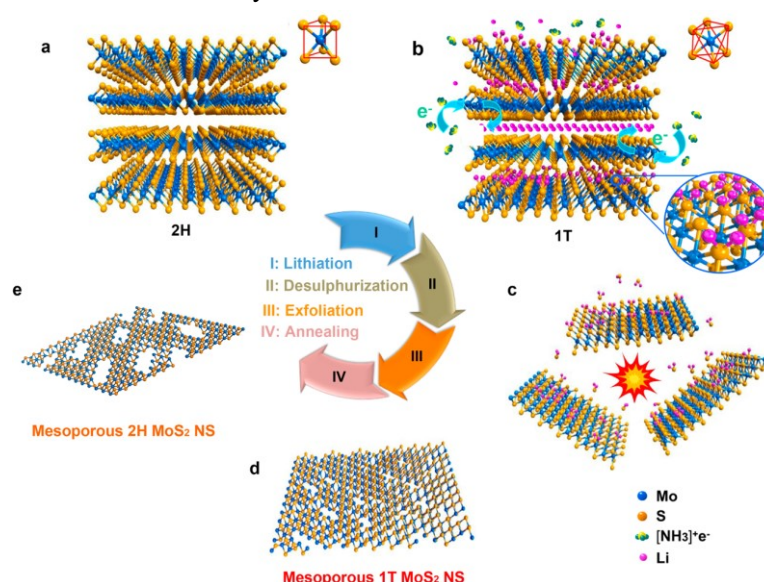


Figure 29. Schematic illustration of the preparation of mesoporous 1T phase MoS₂ nanosheets from bulk MoS₂ (a) by a LAAL process, including lithiation, desulfurization, and exfoliation (steps I, II, and III). Mesoporous 2H phase MoS₂ nanosheets (P-2H-MoS₂, e) can be obtained by a simple thermal annealing process from P-1T-MoS₂ (step IV)¹²¹ (Adapted with permission from ref. 121. Copyright 2016, American Chemical Society.)

As depicted in Figure 29, porous MoS₂ has been synthesized by chemical treatment of MoS₂ in the liquid NH₃ solution under low temperature by Song Jin *et. al.*, Mo and S atoms were etched by highly reactive NH₃ liquid to form nano hole¹²¹. The porosity MoS₂ expose more internal with edge catalytic active sites and facilitate the HER performance.

Carbon substrate support materials like carbon nanofibers¹²²⁻¹²³, carbon cloth^{119, 124}, carbon paper¹²⁵, carbon nanotubes¹²⁶, graphene foam¹²⁷, graphene film¹²⁸, and Si/SiO₂^{90, 129} have been applied in binding with MoS₂ to form heterojunction materials to exhibit strong synergistic effect⁹¹ and improved conductivity¹³⁰. And the porous nanostructure stabilized the electrode as well as the catalyst by timely release the yield H₂, which gives a much higher current density¹³¹.

Mechanism studies in MoS₂ water splitting, under-employed strategies for high performance HER catalysts

Catalytic site

As depict in Figure 30 (a), MoS₂ were predicted to be an active electrocatalyst for water splitting based on theoretical calculation of thermochemical Gibbs energy changes in hydrogen evolution, the results show that adsorption energy is close to zero point which represent the benign adsorption

and desorption process¹³². Then, in the year of 2007, Chorkendorff *et. al.* designed the controlling experiment and make a verification of the edge site catalytic site, they found that the HER performance increase with exposed edge atoms linearly (Figure 30 (b))¹³³. Edge sites, sulfur vacancies, grain boundaries, alien catalytic sites were reaction sites for hydrogen evolution reactions, and Cao *et. al.* make a comparison of the intrinsic HER performance using TOF and Tafel slopes, which are 7.5 s^{-1} (65~75 mV/dec) (edge site), 3.2 s^{-1} (65~85 mV/dec) (sulfur vacancies), 0.1 s^{-1} (120~160 mV/dec) (grain boundaries)⁷⁸. Thomas F. Jaramillo *et. al.* made a detailed catalytic performance study on various intrinsic catalytic sites by TOF index¹³⁴. And catalytic mechanism based on heterojunction engineering, interface engineering, were also studied. As shown in Figure (c), the catalytic mechanism of the sulfur vacancies and undercoordinated Mo were studied⁸⁰. By systematic make samples with S defects with concentration ranging from 0~90 %, the HER performance prone to regulated by two rules, which corresponding to S vacancy and exposed Mo atom.

As depict in Figure (e-f), synergistic effect between Ni(OH)_2 and MoS_2 regulate the reaction route and reduced intermediate energy barrier, and exhibit elevated overall performance by adjust the H^* intermediate adsorption energy ΔG ¹⁰⁵.

Active site

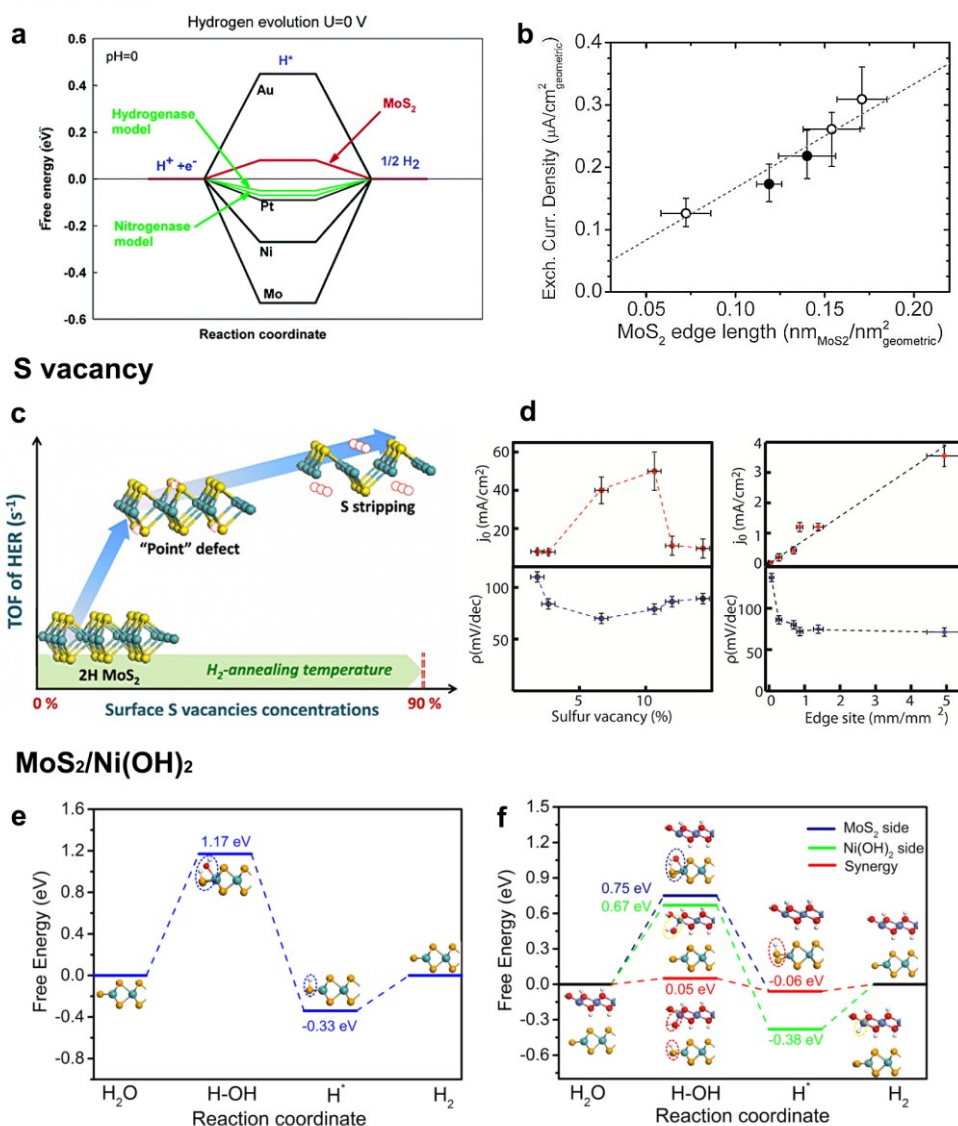


Figure 30. (a). Calculated free energy diagram for hydrogen evolution at a potential $U = 0$ (pH 0)¹³². (Adapted with permission from ref. 132. Copyright 2005, American Chemical Society.) (b) Correlate HER performance to MoS₂ edge site: Exchange current density versus MoS₂ edge length¹³³ (Adapted with permission from ref 133. Copyright 2007, American Association for the Advancement of Science) (c) Correlation between surface S vacancies and catalytic HER's TOF value⁸⁰ (Adapted with permission from ref. 80. Copyright 2019, American Chemical Society.) (d) Exchange current densities (upper) and Tafel slopes of the films as a function of the density of sulfur vacancies (left) and edge (right)⁷⁸ (Adapted with permission from ref. 78. Copyright 2016, American Chemical Society.) (e-f) DFT calculation of free energy diagram for HER by MoS₂/Ni(OH)₂ hybrid catalyst: free energy diagram for HER on the MoS₂ edge (e) and Ni(OH)₂/MoS₂ interface (f)¹⁰⁵ (Adapted with permission from ref. 105. Copyright 2017, Elsevier Ltd.).

Mechanism, Kinetic, and intermediate

To make a better understanding of the mechanism during HER, kinetics and intermediate studies were carried out. To study catalytic reaction on S vacancies, Kye Yeop Kim *et al.* applied multiscale

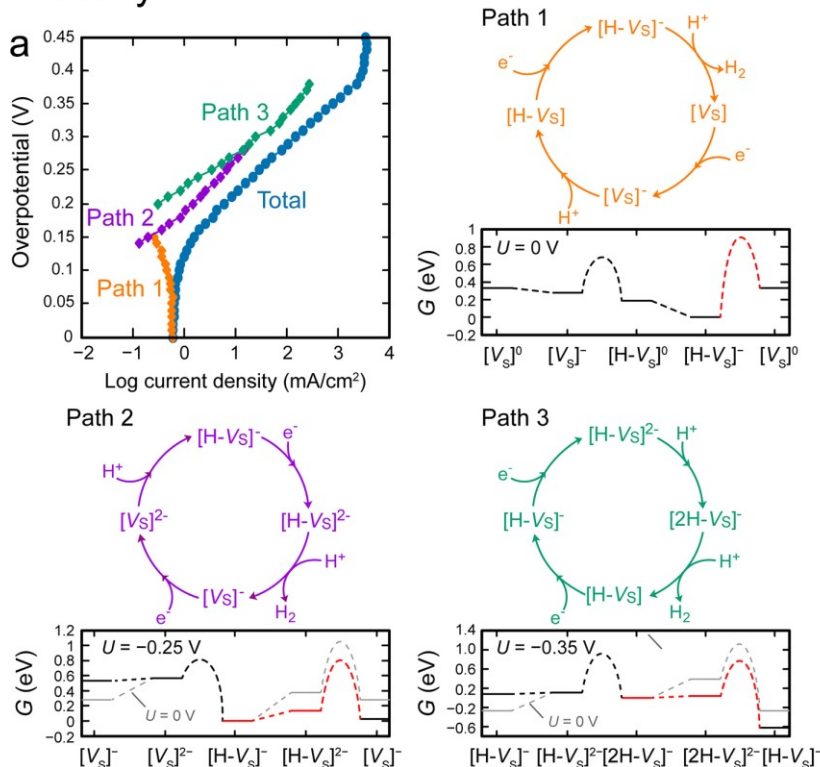
simulation combining *ab initio* calculations and kinetic Monte Carlo (KMC) simulations to examine HER reaction on MoS₂ monolayer S vacancy, the calculation result on TOF and polarization curve agrees well with experimental results, and the author discovered that hyper-reduced states in the HER reaction is playing an important role¹³⁵. When S vacancy site is hyper-reduced with extra electrons by applying overpotential, HER barrier would decrease. Jiang *et al.* make a study to focus on HER performance of 1T-MoS₂, they found that HER can readily take place on the basal plane by Volmer-Heyrovsky route, if Mn, Cr, Cu, Ni, Fe were doped in 1T-MoS₂, better performance can be arrived¹³⁶. And the HER mechanism on “zigzag” and “armchair” 1T-2H interface were examined by DFT simulation, the result show that Volmer-Tafel is more energetically favorable route¹³⁷. While another paper found that on the 1T'-2H interface, the Volmer-Heyrovsky route is more convenient¹³⁸. Kinetic control¹³⁹⁻¹⁴⁰ improvement on mass-transport is achieved by construct 2D channel to facilitate timely reactant supply and rapid gas release. Orbital control⁶⁵ is found by Qian *et al.* to show that it will facilitate water adsorption behavior in C doped MoS₂. Looking forward to theoretical calculation, useful and even instructive information can be arrived¹⁴¹. MoS₂ nanocone arrays were fabricated by SF₆/C₄F₈ plasma assist etching, and the Tafel slope value were decreased with 50 mV dec⁻¹, the results is corresponding to kinetic optimize effect¹⁴².

Key intermediate species and surface bonding structure changes of the catalysts can be identified by *in-situ* XAS characterization method, as shown in Figure 32 (b) that S-S in amorphous surface Mo^{III}-(S-S) were broken to bind to H and form in electrocatalysis procedure¹⁴³. (Evidence from in Situ X-ray Absorption Spectroscopy for the Involvement of Terminal Disulfide in the Reduction of Protons by an Amorphous Molybdenum Sulfide Electrocatalyst).

Electrocatalysis is not just catalysis reactions, conductivity, adsorption and product release, catalytic site, electro-stability all play a role to the overall performance. To get better catalytic performance, taken two or more point into accounts is favorable to arrive better results²⁸.

Mechanism and Kinetics

Vacancy



1T phase

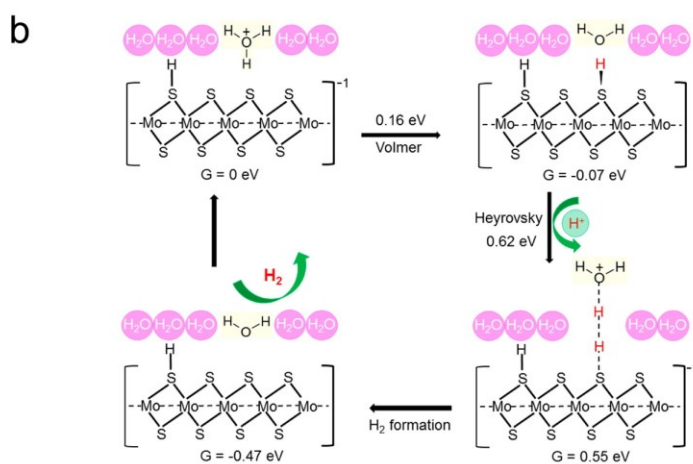


Figure 31. mechanism study on MoS₂ vacancies (a) and 1T phase MoS₂ (b). (a) Tafel plot of major paths in vacancy catalytic site and the detailed pathways of Path 1–3 (The red line is the rate-limiting step and gray lines represent the corresponding path when the potential is 0). Paths 1–3 are the Tafel plots of major paths when overpotential is 0, –0.25, and –0.35 V, respectively¹³⁵. (Adapted with permission from ref. 121. Copyright 2018, American Chemical Society.) (b) Overall reaction mechanism for HER on the surface of 1T MoS₂. Relative free energy (G) values and activation energies (for the Volmer and Heyrovsky steps) are also shown¹³⁶. (Adapted with permission from ref. 135. Copyright 2016, American Chemical Society.)

Mechanism and Kinetics

Amorphous

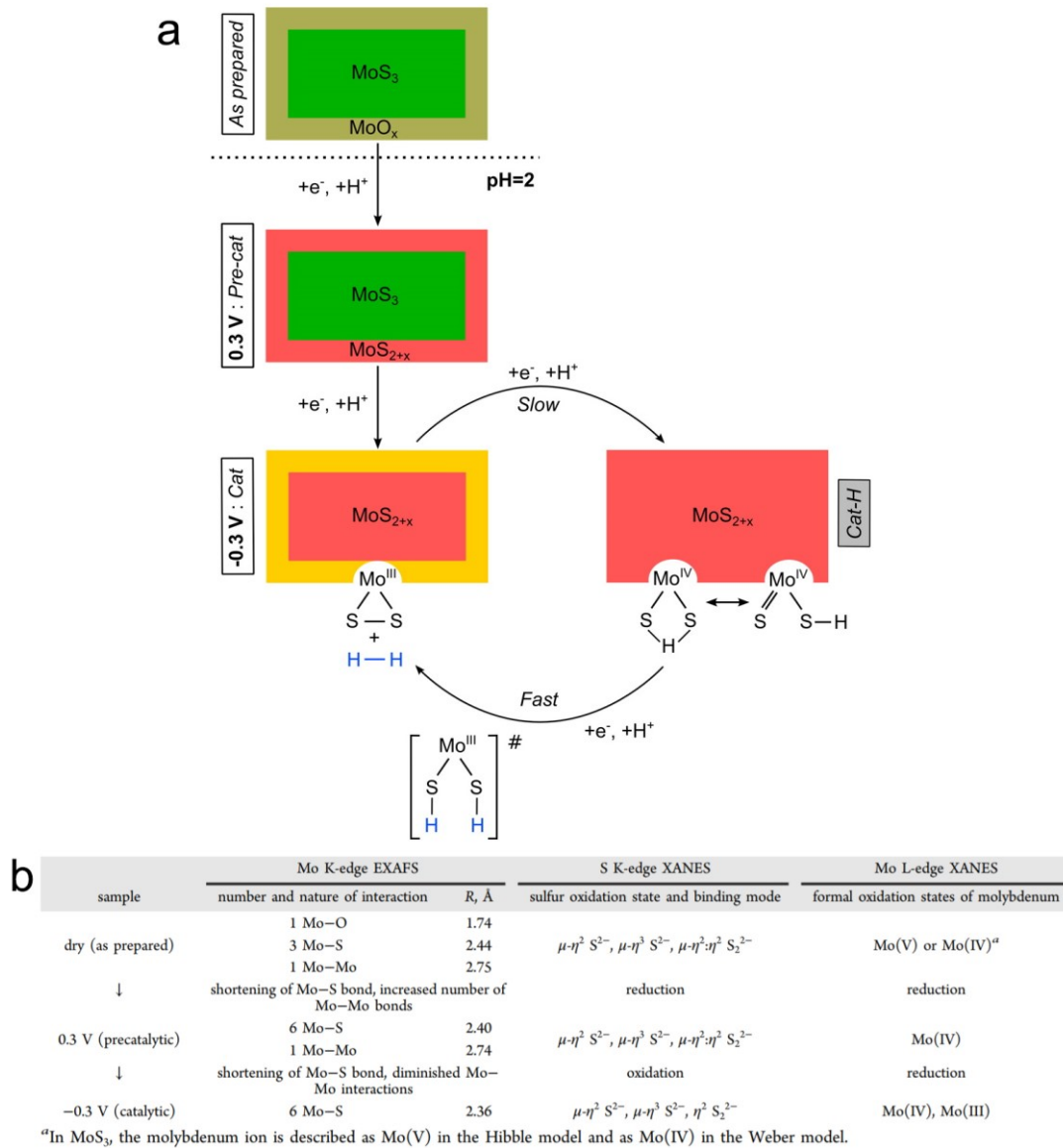


Figure 32. (a) Proposed Changes and Catalytic Cycle for the MoS_x Film as Prepared and at pH = 2 under Pre-Catalytic and Catalytic Conditions (b) the corresponding Spectroscopic Features¹⁴³. (Adapted with permission from ref. 143. Copyright 2015, American Chemical Society.)

Table 1. Typical superior Pt-like HER electrocatalysts

Items	Synthesis Strategies	Synthesis Methods	HER activity	Reference
C-MoS ₂	Non metal doping	Mo ₂ C, 600 °C partial sulfurization	45 mV at 10 mA cm ⁻² (1 M KOH) (close to Pt/C)	Nature Commun. 2019, 10, 1217

NiO-1T MoS ₂	Co-doping		[NiH ₆ Mo ₆ O ₂₄] ⁴⁻ , thioacetamide, carbon fiber paper (180 °C, 24 h)	>80 mA cm ⁻² (better than Pt/C) (1 M KOH)	Nature Commun. 2019, 10, 982
Ni ₂ P/MoS ₂ / N:RGO	Heterojunction, Substrate		NiMoS ₄ , N-RGO (RGO NH ₃ treat at 800 °C), NaH ₂ PO ₂ calcition	>200 mA cm ⁻² (better than Pt/C) (0.5 M H ₂ SO ₄)	Adv. Funct. Mater. 2019, 29, 1809151
Co, Se co- doped MoS ₂	Co-doping, porous structure		SiO ₂ template assist hydrothermal by (NH ₄) ₆ Mo ₇ O ₂₄ ·4H ₂ O, CS ₂ , and Se powder	>208 mA cm ⁻² (better than Pt/C, 0.5 M H ₂ SO ₄)	Nature Commun. 2020, 11, 3315
Co(0)/1T MoS ₂	Basal activation	plane	Cobalt nanodisk and MoS ₂ nanosheet interface reaction under sonication	42 mV (10 mA cm ⁻² , 0.5 M H ₂ SO ₄) Tafel slope 32 mV dec ⁻¹	Nature Commun. 2019, 10, 5231
W- MoS ₂ /MoO ₂ /CNT	Doping, substrate,	porous	(NH ₄) ₆ Mo ₇ O ₂₄ ·4H ₂ O, (NH ₄) ₆ H ₂ W ₁₂ O ₄₀ ·xH ₂ O load onto CNT, then calcite at 400 °C, sulfurization at 550 °C	62 mV (10 mA cm ⁻²), Tafel slope 44 mV dec ⁻¹ ()	J. Mater. Chem. A, 2020,8, 14944- 14954
1L MoS ₂ /Ti/PD MS	7~10 % S vacancy, Ti Substrate effect (low interfacial tunneling barriers)		CVD synthesis of S vacancy-1L MoS ₂ , transfer to Ti substrate	Pt-like performance (0.5 M H ₂ SO ₄), better than Pt/C (> ~7 mA cm ⁻²)	ACS Nano. 2020, 14, 1707-1714

Conclusion:

MoS₂ is a promising substitution HER catalyst for Platinum, for MoS₂ are abundant, non-toxic, and stable during the catalysis reaction. Nano scale engineering like doping, vacancy, defect, edge exposure, phase engineering strategies were demonstrated for adjustment of MoS₂'s intrinsic properties. What's more, heterojunction engineering, interfacial engineering, substrate effect have been developed for elevate MoS₂'s HER performance. Recently, more works have devoted to apply multiple synergistic strategies to achieve better catalytic performance and stability. Accompanied with above strategies, Pt-like activity or even superior activity can be achieved. The catalytic site

and the mechanism for HER reaction were identified and clarified in detail by the theoretical as well as experimental work. Since a wealthy of various TMD materials, MoS₂ and other TMD catalyst with better performance is expected to achieved.

Reference

1. Wang, Z.; Mi, B., Environmental Applications of 2D Molybdenum Disulfide (MoS₂) Nanosheets. *Environmental Science & Technology* **2017**, *51* (15), 8229-8244.
2. Manzeli, S.; Ovchinnikov, D.; Pasquier, D.; Yazyev, O. V.; Kis, A., 2D transition metal dichalcogenides. *Nature Reviews Materials* **2017**, *2* (8), 17033.
3. Hinnemann, B.; Moses, P. G.; Bonde, J.; Jørgensen, K. P.; Nielsen, J. H.; Horch, S.; Chorkendorff, I.; Nørskov, J. K., Biomimetic hydrogen evolution: MoS₂ nanoparticles as catalyst for hydrogen evolution. *J Am Chem Soc* **2005**, *127* (15), 5308-9.
4. Holinski, R.; Gänshelmer, J., A study of the lubricating mechanism of molybdenum disulfide. *Wear* **1972**, *19* (3), 329-342.
5. Chen, Z.; Liu, Y.; Gunsell, S.; Luo, J., Mechanism of Antiwear Property Under High Pressure of Synthetic Oil-Soluble Ultrathin MoS₂ Sheets as Lubricant Additives. *Langmuir* **2018**, *34* (4), 1635-1644.
6. He, Z.; Que, W., Molybdenum disulfide nanomaterials: Structures, properties, synthesis and recent progress on hydrogen evolution reaction. *Applied Materials Today* **2016**, *3*, 23-56.
7. Yang, H.; Kim, S. W.; Chhowalla, M.; Lee, Y. H., Structural and quantum-state phase transitions in van der Waals layered materials. *Nature Physics* **2017**, *13* (10), 931-937.
8. Chhowalla, M.; Shin, H. S.; Eda, G.; Li, L.-J.; Loh, K. P.; Zhang, H., The chemistry of two-dimensional layered transition metal dichalcogenide nanosheets. *Nature Chemistry* **2013**, *5* (4), 263-275.
9. Qian, X.; Liu, J.; Fu, L.; Li, J., Quantum spin Hall effect in two-dimensional transition metal dichalcogenides. *Science* **2014**, *346*, 1344-1347.
10. Wu, C.; Zhang, J.; Tong, X.; Yu, P.; Xu, J.-Y.; Wu, J.; Wang, Z. M.; Lou, J.; Chueh, Y.-L., A Critical Review on Enhancement of Photocatalytic Hydrogen Production by Molybdenum Disulfide: From Growth to Interfacial Activities. *Small* **2019**, *15* (35), 1900578.
11. Lin, Y.-C.; Dumcenco, D. O.; Huang, Y.-S.; Suenaga, K., Atomic mechanism of the semiconducting-to-metallic phase transition in single-layered MoS₂. *Nature Nanotechnology* **2014**, *9* (5), 391-396.
12. Zhao, W.; Pan, J.; Fang, Y.; Che, X.; Wang, D.; Bu, K.; Huang, F., Metastable MoS₂: Crystal Structure, Electronic Band Structure, Synthetic Approach and Intriguing Physical Properties. *Chemistry – A European Journal* **2018**, *24* (60), 15942-15954.
13. Heising, J.; Kanatzidis, M. G., Structure of Restacked MoS₂ and WS₂ Elucidated by Electron Crystallography. *Journal of the American Chemical Society* **1999**, *121* (4), 638-643.
14. Fang, Y.; Hu, X.; Zhao, W.; Pan, J.; Wang, D.; Bu, K.; Mao, Y.; Chu, S.; Liu, P.; Zhai, T.; Huang, F., Structural Determination and Nonlinear Optical Properties of New 1T^{''}-Type MoS₂ Compound. *Journal of the American Chemical Society* **2019**, *141* (2), 790-793.
15. Shang, C.; Fang, Y. Q.; Zhang, Q.; Wang, N. Z.; Wang, Y. F.; Liu, Z.; Lei, B.; Meng, F. B.; Ma, L. K.; Wu, T.; Wang, Z. F.; Zeng, C. G.; Huang, F. Q.; Sun, Z.; Chen, X. H., Superconductivity in the metastable 1T['] and 1T^{''} phases of MoS₂ crystals. *Physical Review B* **2018**, *98* (18), 184513.
16. Yu, Y.; Nam, G.-H.; He, Q.; Wu, X.-J.; Zhang, K.; Yang, Z.; Chen, J.; Ma, Q.; Zhao, M.; Liu, Z.; Ran, F.-

- R.; Wang, X.; Li, H.; Huang, X.; Li, B.; Xiong, Q.; Zhang, Q.; Liu, Z.; Gu, L.; Du, Y.; Huang, W.; Zhang, H., High phase-purity 1T' -MoS₂- and 1T' -MoSe₂-layered crystals. *Nature Chemistry* **2018**, *10* (6), 638-643.
17. Toh, R. J.; Sofer, Z.; Luxa, J.; Sedmidubský, D.; Pumera, M., 3R phase of MoS₂ and WS₂ outperforms the corresponding 2H phase for hydrogen evolution. *Chemical Communications* **2017**, *53* (21), 3054-3057.
18. Zheng, J.; Zhang, H.; Dong, S.; Liu, Y.; Tai Nai, C.; Suk Shin, H.; Young Jeong, H.; Liu, B.; Ping Loh, K., High yield exfoliation of two-dimensional chalcogenides using sodium naphthalenide. *Nature Communications* **2014**, *5* (1), 2995.
19. Liu, Y.-T.; Zhu, X.-D.; Duan, Z.-Q.; Xie, X.-M., Flexible and robust MoS₂-graphene hybrid paper cross-linked by a polymer ligand: a high-performance anode material for thin film lithium-ion batteries. *Chemical Communications* **2013**, *49* (87), 10305-10307.
20. Ejigu, A.; Kinloch, I. A.; Prestat, E.; Dryfe, R. A. W., A simple electrochemical route to metallic phase trilayer MoS₂: evaluation as electrocatalysts and supercapacitors. *Journal of Materials Chemistry A* **2017**, *5* (22), 11316-11330.
21. Nguyen, T. P.; Sohn, W.; Oh, J. H.; Jang, H. W.; Kim, S. Y., Size-Dependent Properties of Two-Dimensional MoS₂ and WS₂. *The Journal of Physical Chemistry C* **2016**, *120* (18), 10078-10085.
22. Eda, G.; Yamaguchi, H.; Voiry, D.; Fujita, T.; Chen, M.; Chhowalla, M., Photoluminescence from Chemically Exfoliated MoS₂. *Nano Letters* **2011**, *11* (12), 5111-5116.
23. Amani, M.; Lien, D.-H.; Kiriya, D.; Xiao, J.; Azcatl, A.; Noh, J.; Madhvapathy, S.; Addou, R.; Kc, S.; Dubey, M.; Cho, K.; Wallace, R.; Lee, S.-c.; He, J. H.; Ager, J.; Zhang, X.; Yablonovitch, E.; Javey, A., Near-unity photoluminescence quantum yield in MoS₂. *Science* **2015**, *350*, 1065-1068.
24. Mouri, S.; Miyauchi, Y.; Matsuda, K., Tunable Photoluminescence of Monolayer MoS₂ via Chemical Doping. *Nano Letters* **2013**, *13* (12), 5944-5948.
25. Deng, S.; Luo, M.; Ai, C.; Zhang, Y.; Liu, B.; Huang, L.; Jiang, Z.; Zhang, Q.; Gu, L.; Lin, S.; Wang, X.; Yu, L.; Wen, J.; Wang, J.; Pan, G.; Xia, X.; Tu, J., Synergistic Doping and Intercalation: Realizing Deep Phase Modulation on MoS₂ Arrays for High-Efficiency Hydrogen Evolution Reaction. *Angewandte Chemie International Edition* **2019**, *58* (45), 16289-16296.
26. Wu, L.; Longo, A.; Dzade, N. Y.; Sharma, A.; Hendrix, M. M. R. M.; Bol, A. A.; de Leeuw, N. H.; Hensen, E. J. M.; Hofmann, J. P., The Origin of High Activity of Amorphous MoS₂ in the Hydrogen Evolution Reaction. *ChemSusChem* **2019**, *12* (19), 4383-4389.
27. Kondekar, N. P.; Boebinger, M. G.; Woods, E. V.; McDowell, M. T., In Situ XPS Investigation of Transformations at Crystallographically Oriented MoS₂ Interfaces. *ACS Applied Materials & Interfaces* **2017**, *9* (37), 32394-32404.
28. Anjum, M. A. R.; Jeong, H. Y.; Lee, M. H.; Shin, H. S.; Lee, J. S., Efficient Hydrogen Evolution Reaction Catalysis in Alkaline Media by All-in-One MoS₂ with Multifunctional Active Sites. *Advanced Materials* **2018**, *30* (20), 1707105.
29. Shi, J.; Yu, P.; Liu, F.; He, P.; Wang, R.; Qin, L.; Zhou, J.; Li, X.; Zhou, J.; Sui, X.; Zhang, S.; Zhang, Y.; Zhang, Q.; Sum, T. C.; Qiu, X.; Liu, Z.; Liu, X., 3R MoS₂ with Broken Inversion Symmetry: A Promising Ultrathin Nonlinear Optical Device. *Advanced Materials* **2017**, *29* (30), 1701486.
30. Hong, J.; Hu, Z.; Probert, M.; Li, K.; Lv, D.; Yang, X.; Gu, L.; Mao, N.; Feng, Q.; Xie, L.; Zhang, J.; Wu, D.; Zhang, Z.; Jin, C.; Ji, W.; Zhang, X.; Yuan, J.; Zhang, Z., Exploring atomic defects in molybdenum disulfide monolayers. *Nature Communications* **2015**, *6* (1), 6293.
31. Nam, G.-H.; He, Q.; Wang, X.; Yu, Y.; Chen, J.; Zhang, K.; Yang, Z.; Hu, D.; Lai, Z.; Li, B.; Xiong, Q.;

Zhang, Q.; Gu, L.; Zhang, H., In-Plane Anisotropic Properties of 1T' -MoS₂ Layers. *Advanced Materials* **2019**, *31* (21), 1807764.

32. Jiao, Y.; Hafez, A. M.; Cao, D.; Mukhopadhyay, A.; Ma, Y.; Zhu, H., Metallic MoS₂ for High Performance Energy Storage and Energy Conversion. *Small* **2018**, *14* (36), 1800640.

33. Li, H.; Zhang, Q.; Yap, C. C. R.; Tay, B. K.; Edwin, T. H. T.; Olivier, A.; Baillargeat, D., From Bulk to Monolayer MoS₂: Evolution of Raman Scattering. *Advanced Functional Materials* **2012**, *22* (7), 1385-1390.

34. Deng, Y.; Ting, L. R. L.; Neo, P. H. L.; Zhang, Y.-J.; Peterson, A. A.; Yeo, B. S., Operando Raman Spectroscopy of Amorphous Molybdenum Sulfide (MoS_x) during the Electrochemical Hydrogen Evolution Reaction: Identification of Sulfur Atoms as Catalytically Active Sites for H⁺ Reduction. *ACS Catalysis* **2016**, *6* (11), 7790-7798.

35. Huang, T.-X.; Cong, X.; Wu, S.-S.; Lin, K.-Q.; Yao, X.; He, Y.-H.; Wu, J.-B.; Bao, Y.-F.; Huang, S.-C.; Wang, X.; Tan, P.-H.; Ren, B., Probing the edge-related properties of atomically thin MoS₂ at nanoscale. *Nature Communications* **2019**, *10* (1), 5544.

36. Zeleke, T. S.; Tsai, M.-C.; Weret, M. A.; Huang, C.-J.; Birhanu, M. K.; Liu, T.-C.; Huang, C.-P.; Soo, Y.-L.; Yang, Y.-W.; Su, W.-N.; Hwang, B.-J., Immobilized Single Molecular Molybdenum Disulfide on Carbonized Polyacrylonitrile for Hydrogen Evolution Reaction. *ACS Nano* **2019**, *13* (6), 6720-6729.

37. Wang, M.; Árnadóttir, L.; Xu, Z. J.; Feng, Z., In Situ X-ray Absorption Spectroscopy Studies of Nanoscale Electrocatalysts. *Nano-Micro Letters* **2019**, *11* (1), 47.

38. Gao, M.-R.; Chan, M. K. Y.; Sun, Y., Edge-terminated molybdenum disulfide with a 9.4-Å interlayer spacing for electrochemical hydrogen production. *Nature Communications* **2015**, *6* (1), 7493.

39. Yang, S.-Z.; Gong, Y.; Manchanda, P.; Zhang, Y.-Y.; Ye, G.; Chen, S.; Song, L.; Pantelides, S. T.; Ajayan, P. M.; Chisholm, M. F.; Zhou, W., Rhenium-Doped and Stabilized MoS₂ Atomic Layers with Basal-Plane Catalytic Activity. *Advanced Materials* **2018**, *30* (51), 1803477.

40. Zhang, X.; Zhou, F.; Zhang, S.; Liang, Y.; Wang, R., Engineering MoS₂ Basal Planes for Hydrogen Evolution via Synergistic Ruthenium Doping and Nanocarbon Hybridization. *Advanced Science* **2019**, *6* (10), 1900090.

41. Qi, K.; Cui, X.; Gu, L.; Yu, S.; Fan, X.; Luo, M.; Xu, S.; Li, N.; Zheng, L.; Zhang, Q.; Ma, J.; Gong, Y.; Lv, F.; Wang, K.; Huang, H.; Zhang, W.; Guo, S.; Zheng, W.; Liu, P., Single-atom cobalt array bound to distorted 1T MoS₂ with ensemble effect for hydrogen evolution catalysis. *Nature Communications* **2019**, *10* (1), 5231.

42. Luo, Y.; Zhang, S.; Pan, H.; Xiao, S.; Guo, Z.; Tang, L.; Khan, U.; Ding, B.-F.; Li, M.; Cai, Z.; Zhao, Y.; Lv, W.; Feng, Q.; Zou, X.; Lin, J.; Cheng, H.-M.; Liu, B., Unsaturated Single Atoms on Monolayer Transition Metal Dichalcogenides for Ultrafast Hydrogen Evolution. *ACS Nano* **2020**, *14* (1), 767-776.

43. Kim, M.; Anjum, M. A. R.; Lee, M.; Lee, B. J.; Lee, J. S., Activating MoS₂ Basal Plane with Ni₂P Nanoparticles for Pt-Like Hydrogen Evolution Reaction in Acidic Media. *Advanced Functional Materials* **2019**, *29* (10), 1809151.

44. Zhao, S.; Jin, R.; Song, Y.; Zhang, H.; House, S. D.; Yang, J. C.; Jin, R., Atomically Precise Gold Nanoclusters Accelerate Hydrogen Evolution over MoS₂ Nanosheets: The Dual Interfacial Effect. *Small* **2017**, *13* (43), 1701519.

45. Kim, Y.; Jackson, D. H. K.; Lee, D.; Choi, M.; Kim, T.-W.; Jeong, S.-Y.; Chae, H.-J.; Kim, H. W.; Park, N.; Chang, H.; Kuech, T. F.; Kim, H. J., In Situ Electrochemical Activation of Atomic Layer Deposition Coated MoS₂ Basal Planes for Efficient Hydrogen Evolution Reaction. *Advanced Functional Materials* **2017**, *27* (34), 1701825.

46. Huang, X.; Leng, M.; Xiao, W.; Li, M.; Ding, J.; Tan, T. L.; Lee, W. S. V.; Xue, J., Activating Basal Planes and S-Terminated Edges of MoS₂ toward More Efficient Hydrogen Evolution. *Advanced Functional Materials* **2017**, *27* (6), 1604943.
47. Jiménez Sandoval, S.; Yang, D.; Frindt, R. F.; Irwin, J. C., Raman study and lattice dynamics of single molecular layers of MoS_2 . *Physical Review B* **1991**, *44* (8), 3955-3962.
48. Shang, B.; Cui, X.; Jiao, L.; Qi, K.; Wang, Y.; Fan, J.; Yue, Y.; Wang, H.; Bao, Q.; Fan, X.; Wei, S.; Song, W.; Cheng, Z.; Guo, S.; Zheng, W., Lattice Mismatch-Induced Ultrastable 1T-Phase MoS₂-Pd/Au for Plasmon-Enhanced Hydrogen Evolution. *Nano Letters* **2019**, *19* (5), 2758-2764.
49. Wei, S.; Cui, X.; Xu, Y.; Shang, B.; Zhang, Q.; Gu, L.; Fan, X.; Zheng, L.; Hou, C.; Huang, H.; Wen, S.; Zheng, W., Iridium-Triggered Phase Transition of MoS₂ Nanosheets Boosts Overall Water Splitting in Alkaline Media. *ACS Energy Letters* **2019**, *4* (1), 368-374.
50. Ding, W.; Hu, L.; Dai, J.; Tang, X.; Wei, R.; Sheng, Z.; Liang, C.; Shao, D.; Song, W.; Liu, Q.; Chen, M.; Zhu, X.; Chou, S.; Zhu, X.; Chen, Q.; Sun, Y.; Dou, S. X., Highly Ambient-Stable 1T-MoS₂ and 1T-WS₂ by Hydrothermal Synthesis under High Magnetic Fields. *ACS Nano* **2019**, *13* (2), 1694-1702.
51. Liu, Q.; Li, X.; He, Q.; Khalil, A.; Liu, D.; Xiang, T.; Wu, X.; Song, L., Gram-Scale Aqueous Synthesis of Stable Few-Layered 1T-MoS₂: Applications for Visible-Light-Driven Photocatalytic Hydrogen Evolution. *Small* **2015**, *11* (41), 5556-5564.
52. Tsai, C.; Chan, K.; Nørskov, J. K.; Abild-Pedersen, F., Rational design of MoS₂ catalysts: tuning the structure and activity via transition metal doping. *Catalysis Science & Technology* **2015**, *5* (1), 246-253.
53. Deng, J.; Li, H.; Xiao, J.; Tu, Y.; Deng, D.; Yang, H.; Tian, H.; Li, J.; Ren, P.; Bao, X., Triggering the electrocatalytic hydrogen evolution activity of the inert two-dimensional MoS₂ surface via single-atom metal doping. *Energy & Environmental Science* **2015**, *8* (5), 1594-1601.
54. Enyashin, A. N.; Yadgarov, L.; Houben, L.; Popov, I.; Weidenbach, M.; Tenne, R.; Bar-Sadan, M.; Seifert, G., New Route for Stabilization of 1T-WS₂ and MoS₂ Phases. *The Journal of Physical Chemistry C* **2011**, *115* (50), 24586-24591.
55. Shi, Y.; Zhou, Y.; Yang, D.-R.; Xu, W.-X.; Wang, C.; Wang, F.-B.; Xu, J.-J.; Xia, X.-H.; Chen, H.-Y., Energy Level Engineering of MoS₂ by Transition-Metal Doping for Accelerating Hydrogen Evolution Reaction. *Journal of the American Chemical Society* **2017**, *139* (43), 15479-15485.
56. Xue, J.-Y.; Li, F.-L.; Zhao, Z.-Y.; Li, C.; Ni, C.-Y.; Gu, H.-W.; Young, D. J.; Lang, J.-P., In Situ Generation of Bifunctional Fe-Doped MoS₂ Nanocanopies for Efficient Electrocatalytic Water Splitting. *Inorganic Chemistry* **2019**, *58* (16), 11202-11209.
57. Dai, X.; Du, K.; Li, Z.; Liu, M.; Ma, Y.; Sun, H.; Zhang, X.; Yang, Y., Co-Doped MoS₂ Nanosheets with the Dominant CoMoS Phase Coated on Carbon as an Excellent Electrocatalyst for Hydrogen Evolution. *ACS Applied Materials & Interfaces* **2015**, *7* (49), 27242-27253.
58. Li, C.; Zhao, S.; Zhu, K.; Wang, B.; Wang, E.; Luo, Y.; He, L.; Wang, J.; Jiang, K.; Fan, S.; Li, J.; Liu, K., Flexible and free-standing hetero-electrocatalyst of high-valence-cation doped MoS₂/MoO₂/CNT foam with synergistically enhanced hydrogen evolution reaction catalytic activity. *Journal of Materials Chemistry A* **2020**.
59. Xiao, W.; Liu, P.; Zhang, J.; Song, W.; Feng, Y. P.; Gao, D.; Ding, J., Dual-Functional N Dopants in Edges and Basal Plane of MoS₂ Nanosheets Toward Efficient and Durable Hydrogen Evolution. *Advanced Energy Materials* **2017**, *7* (7), 1602086.
60. Xie, J.; Zhang, J.; Li, S.; Grote, F.; Zhang, X.; Zhang, H.; Wang, R.; Lei, Y.; Pan, B.; Xie, Y., Controllable Disorder Engineering in Oxygen-Incorporated MoS₂ Ultrathin Nanosheets for Efficient Hydrogen Evolution. *Journal of the American Chemical Society* **2013**, *135* (47), 17881-17888.

61. Pető, J.; Ollár, T.; Vancsó, P.; Popov, Z. I.; Magda, G. Z.; Dobrik, G.; Hwang, C.; Sorokin, P. B.; Tapasztó, L., Spontaneous doping of the basal plane of MoS₂ single layers through oxygen substitution under ambient conditions. *Nature Chemistry* **2018**, *10* (12), 1246-1251.
62. Gong, Q.; Cheng, L.; Liu, C.; Zhang, M.; Feng, Q.; Ye, H.; Zeng, M.; Xie, L.; Liu, Z.; Li, Y., Ultrathin MoS₂(1-x)Se_{2x} Alloy Nanoflakes For Electrocatalytic Hydrogen Evolution Reaction. *ACS Catalysis* **2015**, *5* (4), 2213-2219.
63. Ye, R.; del Angel-Vicente, P.; Liu, Y.; Arellano-Jimenez, M. J.; Peng, Z.; Wang, T.; Li, Y.; Yakobson, B. I.; Wei, S.-H.; Yacaman, M. J.; Tour, J. M., High-Performance Hydrogen Evolution from MoS₂(1-x)P_x Solid Solution. *Advanced Materials* **2016**, *28* (7), 1427-1432.
64. Liu, P.; Zhu, J.; Zhang, J.; Xi, P.; Tao, K.; Gao, D.; Xue, D., P Dopants Triggered New Basal Plane Active Sites and Enlarged Interlayer Spacing in MoS₂ Nanosheets toward Electrocatalytic Hydrogen Evolution. *ACS Energy Letters* **2017**, *2* (4), 745-752.
65. Zang, Y.; Niu, S.; Wu, Y.; Zheng, X.; Cai, J.; Ye, J.; Xie, Y.; Liu, Y.; Zhou, J.; Zhu, J.; Liu, X.; Wang, G.; Qian, Y., Tuning orbital orientation endows molybdenum disulfide with exceptional alkaline hydrogen evolution capability. *Nature Communications* **2019**, *10* (1), 1217.
66. Zheng, Z.; Yu, L.; Gao, M.; Chen, X.; Zhou, W.; Ma, C.; Wu, L.; Zhu, J.; Meng, X.; Hu, J.; Tu, Y.; Wu, S.; Mao, J.; Tian, Z.; Deng, D., Boosting hydrogen evolution on MoS₂ via co-confining selenium in surface and cobalt in inner layer. *Nature Communications* **2020**, *11* (1), 3315.
67. Huang, Y.; Sun, Y.; Zheng, X.; Aoki, T.; Pattengale, B.; Huang, J.; He, X.; Bian, W.; Younan, S.; Williams, N.; Hu, J.; Ge, J.; Pu, N.; Yan, X.; Pan, X.; Zhang, L.; Wei, Y.; Gu, J., Atomically engineering activation sites onto metallic 1T-MoS₂ catalysts for enhanced electrochemical hydrogen evolution. *Nature Communications* **2019**, *10* (1), 982.
68. Xiong, Q.; Zhang, X.; Wang, H.; Liu, G.; Wang, G.; Zhang, H.; Zhao, H., One-step synthesis of cobalt-doped MoS₂ nanosheets as bifunctional electrocatalysts for overall water splitting under both acidic and alkaline conditions. *Chemical Communications* **2018**, *54* (31), 3859-3862.
69. Sun, T.; Wang, J.; Chi, X.; Lin, Y.; Chen, Z.; Ling, X.; Qiu, C.; Xu, Y.; Song, L.; Chen, W.; Su, C., Engineering the Electronic Structure of MoS₂ Nanorods by N and Mn Dopants for Ultra-Efficient Hydrogen Production. *ACS Catalysis* **2018**, *8* (8), 7585-7592.
70. Liu, J.; Wang, Z.; Li, J.; Cao, L.; Lu, Z.; Zhu, D., Structure Engineering of MoS₂ via Simultaneous Oxygen and Phosphorus Incorporation for Improved Hydrogen Evolution. *Small* **2020**, *16* (4), 1905738.
71. Zhu, T.; Ding, J.; Shao, Q.; Qian, Y.; Huang, X., P,Se-Codoped MoS₂ Nanosheets as Accelerated Electrocatalysts for Hydrogen Evolution. *ChemCatChem* **2019**, *11* (2), 689-692.
72. Wang, Y.; Liu, S.; Hao, X.; Zhou, J.; Song, D.; Wang, D.; Hou, L.; Gao, F., Fluorine- and Nitrogen-Codoped MoS₂ with a Catalytically Active Basal Plane. *ACS Applied Materials & Interfaces* **2017**, *9* (33), 27715-27719.
73. Bai, F.; Xu, L.; Zhai, X.; Chen, X.; Yang, W., Vacancy in Ultrathin 2D Nanomaterials toward Sustainable Energy Application. *Advanced Energy Materials* **2020**, *10* (11), 1902107.
74. Tsai, C.; Li, H.; Park, S.; Park, J.; Han, H. S.; Nørskov, J. K.; Zheng, X.; Abild-Pedersen, F., Electrochemical generation of sulfur vacancies in the basal plane of MoS₂ for hydrogen evolution. *Nature Communications* **2017**, *8* (1), 15113.
75. Ye, G.; Gong, Y.; Lin, J.; Li, B.; He, Y.; Pantelides, S. T.; Zhou, W.; Vajtai, R.; Ajayan, P. M., Defects Engineered Monolayer MoS₂ for Improved Hydrogen Evolution Reaction. *Nano Letters* **2016**, *16* (2), 1097-1103.
76. Wang, Z.; Li, Q.; Xu, H.; Dahl-Petersen, C.; Yang, Q.; Cheng, D.; Cao, D.; Besenbacher, F.; Lauritsen,

- J. V.; Helveg, S.; Dong, M., Controllable etching of MoS₂ basal planes for enhanced hydrogen evolution through the formation of active edge sites. *Nano Energy* **2018**, *49*, 634-643.
77. Huang, Y.; Nielsen, R. J.; Goddard, W. A., Reaction Mechanism for the Hydrogen Evolution Reaction on the Basal Plane Sulfur Vacancy Site of MoS₂ Using Grand Canonical Potential Kinetics. *Journal of the American Chemical Society* **2018**, *140* (48), 16773-16782.
78. Li, G.; Zhang, D.; Qiao, Q.; Yu, Y.; Peterson, D.; Zafar, A.; Kumar, R.; Curtarolo, S.; Hunte, F.; Shannon, S.; Zhu, Y.; Yang, W.; Cao, L., All The Catalytic Active Sites of MoS₂ for Hydrogen Evolution. *Journal of the American Chemical Society* **2016**, *138* (51), 16632-16638.
79. Wang, X.; Zhang, Y.; Si, H.; Zhang, Q.; Wu, J.; Gao, L.; Wei, X.; Sun, Y.; Liao, Q.; Zhang, Z.; Ammarah, K.; Gu, L.; Kang, Z.; Zhang, Y., Single-Atom Vacancy Defect to Trigger High-Efficiency Hydrogen Evolution of MoS₂. *Journal of the American Chemical Society* **2020**, *142* (9), 4298-4308.
80. Li, L.; Qin, Z.; Ries, L.; Hong, S.; Michel, T.; Yang, J.; Salameh, C.; Bechelany, M.; Miele, P.; Kaplan, D.; Chhowalla, M.; Voiry, D., Role of Sulfur Vacancies and Undercoordinated Mo Regions in MoS₂ Nanosheets toward the Evolution of Hydrogen. *ACS Nano* **2019**, *13* (6), 6824-6834.
81. Wu, W.; Niu, C.-Y.; Wei, C.; Li, C.; Xu, Q., Activation of MoS₂ Basal Planes for Hydrogen Evolution through Zinc. *Angewandte Chemie International Edition* **2019**, *58*.
82. Li, H.; Tsai, C.; Koh, A. L.; Cai, L.; Contryman, A. W.; Fragapane, A. H.; Zhao, J.; Han, H. S.; Manoharan, H. C.; Abild-Pedersen, F.; Nørskov, J. K.; Zheng, X., Activating and optimizing MoS₂ basal planes for hydrogen evolution through the formation of strained sulphur vacancies. *Nature Materials* **2016**, *15* (1), 48-53.
83. Ouyang, Y.; Ling, C.; Chen, Q.; Wang, Z.; Shi, L.; Wang, J., Activating Inert Basal Planes of MoS₂ for Hydrogen Evolution Reaction through the Formation of Different Intrinsic Defects. *Chemistry of Materials* **2016**, *28* (12), 4390-4396.
84. Benavente, E.; Santa Ana, M. A.; Mendizábal, F.; González, G., Intercalation chemistry of molybdenum disulfide. *Coordination Chemistry Reviews* **2002**, *224* (1), 87-109.
85. Wang, X.; Xing, W.; Feng, X.; Song, L.; Hu, Y., MoS₂/Polymer Nanocomposites: Preparation, Properties, and Applications. *Polymer Reviews* **2017**, *57* (3), 440-466.
86. Rasamani, K. D.; Alimohammadi, F.; Sun, Y., Interlayer-expanded MoS₂. *Materials Today* **2017**, *20* (2), 83-91.
87. Liang, Y.; Yoo, H. D.; Li, Y.; Shuai, J.; Calderon, H. A.; Robles Hernandez, F. C.; Grabow, L. C.; Yao, Y., Interlayer-Expanded Molybdenum Disulfide Nanocomposites for Electrochemical Magnesium Storage. *Nano Letters* **2015**, *15* (3), 2194-2202.
88. Tang, Y.-J.; Wang, Y.; Wang, X.-L.; Li, S.-L.; Huang, W.; Dong, L.-Z.; Liu, C.-H.; Li, Y.-F.; Lan, Y.-Q., Molybdenum Disulfide/Nitrogen-Doped Reduced Graphene Oxide Nanocomposite with Enlarged Interlayer Spacing for Electrocatalytic Hydrogen Evolution. *Advanced Energy Materials* **2016**, *6* (12), 1600116.
89. Zhu, H.; Du, M.; Zhang, M.; Zou, M.; Yang, T.; Fu, Y.; Yao, J., The design and construction of 3D rose-petal-shaped MoS₂ hierarchical nanostructures with structure-sensitive properties. *Journal of Materials Chemistry A* **2014**, *2* (21), 7680-7685.
90. Kong, D.; Wang, H.; Cha, J. J.; Pasta, M.; Koski, K. J.; Yao, J.; Cui, Y., Synthesis of MoS₂ and MoSe₂ Films with Vertically Aligned Layers. *Nano Letters* **2013**, *13* (3), 1341-1347.
91. Zhang, Z.; Wang, Y.; Leng, X.; Crespi, V. H.; Kang, F.; Lv, R., Controllable Edge Exposure of MoS₂ for Efficient Hydrogen Evolution with High Current Density. *ACS Applied Energy Materials* **2018**, *1* (3), 1268-1275.

92. Wang, W.; Zhu, S.; Cao, Y.; Tao, Y.; Li, X.; Pan, D.; Phillips, D. L.; Zhang, D.; Chen, M.; Li, G.; Li, H., Edge-Enriched Ultrathin MoS₂ Embedded Yolk-Shell TiO₂ with Boosted Charge Transfer for Superior Photocatalytic H₂ Evolution. *Advanced Functional Materials* **2019**, *29* (36), 1901958.
93. Tsai, C.; Abild-Pedersen, F.; Nørskov, J. K., Tuning the MoS₂ Edge-Site Activity for Hydrogen Evolution via Support Interactions. *Nano Letters* **2014**, *14* (3), 1381-1387.
94. Li, G.; Chen, Z.; Li, Y.; Zhang, D.; Yang, W.; Liu, Y.; Cao, L., Engineering Substrate Interaction To Improve Hydrogen Evolution Catalysis of Monolayer MoS₂ Films beyond Pt. *ACS Nano* **2020**, *14* (2), 1707-1714.
95. Morales-Guio, C. G.; Hu, X., Amorphous Molybdenum Sulfides as Hydrogen Evolution Catalysts. *Accounts of Chemical Research* **2014**, *47* (8), 2671-2681.
96. Benck, J. D.; Chen, Z.; Kuritzky, L. Y.; Forman, A. J.; Jaramillo, T. F., Amorphous Molybdenum Sulfide Catalysts for Electrochemical Hydrogen Production: Insights into the Origin of their Catalytic Activity. *ACS Catalysis* **2012**, *2* (9), 1916-1923.
97. Lee, S. C.; Benck, J. D.; Tsai, C.; Park, J.; Koh, A. L.; Abild-Pedersen, F.; Jaramillo, T. F.; Sinclair, R., Chemical and Phase Evolution of Amorphous Molybdenum Sulfide Catalysts for Electrochemical Hydrogen Production. *ACS Nano* **2016**, *10* (1), 624-632.
98. Tran, P. D.; Tran, Thu V.; Orio, M.; Torelli, S.; Truong, Q. D.; Nayuki, K.; Sasaki, Y.; Chiam, Sing Y.; Yi, R.; Honma, I.; Barber, J.; Artero, V., Coordination polymer structure and revisited hydrogen evolution catalytic mechanism for amorphous molybdenum sulfide. *Nature Materials* **2016**, *15* (6), 640-646.
99. Zhu, J.; Wang, Z.-C.; Dai, H.; Wang, Q.; Yang, R.; Yu, H.; Liao, M.; Zhang, J.; Chen, W.; Wei, Z.; Li, N.; Du, L.; Shi, D.; Wang, W.; Zhang, L.; Jiang, Y.; Zhang, G., Boundary activated hydrogen evolution reaction on monolayer MoS₂. *Nature Communications* **2019**, *10* (1), 1348.
100. Peng, R.; Liang, L.; Hood, Z. D.; Boulesbaa, A.; Puzos, A.; Levlev, A. V.; Come, J.; Ovchinnikova, O. S.; Wang, H.; Ma, C.; Chi, M.; Sumpter, B. G.; Wu, Z., In-Plane Heterojunctions Enable Multiphase Two-Dimensional (2D) MoS₂ Nanosheets As Efficient Photocatalysts for Hydrogen Evolution from Water Reduction. *ACS Catalysis* **2016**, *6* (10), 6723-6729.
101. Dong, Y.; Chen, S.-Y.; Lu, Y.; Xiao, Y.-X.; Hu, J.; Wu, S.-M.; Deng, Z.; Tian, G.; Chang, G.; Li, J.; Lenaerts, S.; Yang, X.-Y., Hierarchical MoS₂@TiO₂ Heterojunctions for Enhanced Photocatalytic Performance and Electrocatalytic Hydrogen Evolution. *Chemistry - An Asian Journal* **2018**, *13*.
102. Liu, P.; Yan, J.; Mao, J.; Li, J.; Liang, D.; Song, W., In-plane intergrowth CoS₂/MoS₂ nanosheets: binary metal-organic framework evolution and efficient alkaline HER electrocatalysis. *Journal of Materials Chemistry A* **2020**, *8* (22), 11435-11441.
103. Hu, J.; Zhang, C.; Zhang, Y.; Yang, B.; Qi, Q.; Sun, M.; Zi, F.; Leung, M. K. H.; Huang, B., Interface Modulation of MoS₂/Metal Oxide Heterostructures for Efficient Hydrogen Evolution Electrocatalysis. *Small* *n/a* (n/a), 2002212.
104. Chen, W.; Gu, J.; Du, Y.; Song, F.; Bu, F.; Li, J.; Yuan, Y.; Luo, R.; Liu, Q.; Zhang, D., Achieving Rich and Active Alkaline Hydrogen Evolution Heterostructures via Interface Engineering on 2D 1T-MoS₂ Quantum Sheets. *Advanced Functional Materials* **2020**, *30* (25), 2000551.
105. Zhang, B.; Liu, J.; Wang, J.; Ruan, Y.; Ji, X.; Xu, K.; Chen, C.; Wan, H.; Miao, L.; Jiang, J., Interface engineering: The Ni(OH)₂/MoS₂ heterostructure for highly efficient alkaline hydrogen evolution. *Nano Energy* **2017**, *37*, 74-80.
106. Luo, Y.; Li, X.; Cai, X.; Zou, X.; Kang, F.; Cheng, H.-M.; Liu, B., Two-Dimensional MoS₂ Confined Co(OH)₂ Electrocatalysts for Hydrogen Evolution in Alkaline Electrolytes. *ACS Nano* **2018**, *12* (5), 4565-4573.

107. Hu, J.; Zhang, C.; Jiang, L.; Lin, H.; An, Y.; Zhou, D.; Leung, M. K. H.; Yang, S., Nanohybridization of MoS₂ with Layered Double Hydroxides Efficiently Synergizes the Hydrogen Evolution in Alkaline Media. *Joule* **2017**, *1* (2), 383-393.
108. Gao, M.-R.; Liang, J.-X.; Zheng, Y.-R.; Xu, Y.-F.; Jiang, J.; Gao, Q.; Li, J.; Yu, S.-H., An efficient molybdenum disulfide/cobalt diselenide hybrid catalyst for electrochemical hydrogen generation. *Nature Communications* **2015**, *6* (1), 5982.
109. Attanayake, N. H.; Abeyweera, S. C.; Thenuwara, A. C.; Anasori, B.; Gogotsi, Y.; Sun, Y.; Strongin, D. R., Vertically aligned MoS₂ on Ti₃C₂ (MXene) as an improved HER catalyst. *Journal of Materials Chemistry A* **2018**, *6* (35), 16882-16889.
110. Yu, M.; Zhao, S.; Feng, H.; Hu, L.; Zhang, X.; Zeng, Y.; Tong, Y.; Lu, X., Engineering Thin MoS₂ Nanosheets on TiN Nanorods: Advanced Electrochemical Capacitor Electrode and Hydrogen Evolution Electrocatalyst. *ACS Energy Letters* **2017**, *2* (8), 1862-1868.
111. Wu, A.; Tian, C.; Yan, H.; Jiao, Y.; Yan, Q.; Yang, G.; Fu, H., Hierarchical MoS₂@MoP core-shell heterojunction electrocatalysts for efficient hydrogen evolution reaction over a broad pH range. *Nanoscale* **2016**, *8* (21), 11052-11059.
112. Xu, J.; Cui, J.; Guo, C.; Zhao, Z.; Jiang, R.; Xu, S.; Zhuang, Z.; Huang, Y.; Wang, L.; Li, Y., Ultrasmall Cu₇S₄@MoS₂ Hetero-Nanoframes with Abundant Active Edge Sites for Ultrahigh-Performance Hydrogen Evolution. *Angewandte Chemie International Edition* **2016**, *55* (22), 6502-6505.
113. Jiao, Y.; Mukhopadhyay, A.; Ma, Y.; Yang, L.; Hafez, A. M.; Zhu, H., Ion Transport Nanotube Assembled with Vertically Aligned Metallic MoS₂ for High Rate Lithium-Ion Batteries. *Advanced Energy Materials* **2018**, *8* (15), 1702779.
114. Lv, Z.; Mahmood, N.; Tahir, M.; Pan, L.; Zhang, X.; Zou, J.-J., Fabrication of zero to three dimensional nanostructured molybdenum sulfides and their electrochemical and photocatalytic applications. *Nanoscale* **2016**, *8* (43), 18250-18269.
115. Ding, J.; Zhou, Y.; Li, Y.; Guo, S.; Huang, X., MoS₂ Nanosheet Assembling Superstructure with a Three-Dimensional Ion Accessible Site: A New Class of Bifunctional Materials for Batteries and Electrocatalysis. *Chemistry of Materials* **2016**, *28* (7), 2074-2080.
116. Ren, X.; Pang, L.; Zhang, Y.; Ren, X.; Fan, H.; Liu, S., One-step hydrothermal synthesis of monolayer MoS₂ quantum dots for highly efficient electrocatalytic hydrogen evolution. *Journal of Materials Chemistry A* **2015**, *3* (20), 10693-10697.
117. Kibsgaard, J.; Chen, Z.; Reinecke, B. N.; Jaramillo, T. F., Engineering the surface structure of MoS₂ to preferentially expose active edge sites for electrocatalysis. *Nature Materials* **2012**, *11* (11), 963-969.
118. Guo, B.; Yu, K.; Li, H.; Song, H.; Zhang, Y.; Lei, X.; Fu, H.; Tan, Y.; Zhu, Z., Hollow Structured Micro/Nano MoS₂ Spheres for High Electrocatalytic Activity Hydrogen Evolution Reaction. *ACS Applied Materials & Interfaces* **2016**, *8* (8), 5517-5525.
119. Zhang, N.; Gan, S.; Wu, T.; Ma, W.; Han, D.; Niu, L., Growth Control of MoS₂ Nanosheets on Carbon Cloth for Maximum Active Edges Exposed: An Excellent Hydrogen Evolution 3D Cathode. *ACS Applied Materials & Interfaces* **2015**, *7* (22), 12193-12202.
120. Seo, B.; Jung, G. Y.; Sa, Y. J.; Jeong, H. Y.; Cheon, J. Y.; Lee, J. H.; Kim, H. Y.; Kim, J. C.; Shin, H. S.; Kwak, S. K.; Joo, S. H., Monolayer-Precision Synthesis of Molybdenum Sulfide Nanoparticles and Their Nanoscale Size Effects in the Hydrogen Evolution Reaction. *ACS Nano* **2015**, *9* (4), 3728-3739.
121. Yin, Y.; Han, J.; Zhang, Y.; Zhang, X.; Xu, P.; Yuan, Q.; Samad, L.; Wang, X.; Wang, Y.; Zhang, Z.; Zhang, P.; Cao, X.; Song, B.; Jin, S., Contributions of Phase, Sulfur Vacancies, and Edges to the Hydrogen Evolution Reaction Catalytic Activity of Porous Molybdenum Disulfide Nanosheets. *Journal of the*

American Chemical Society **2016**, *138* (25), 7965-7972.

122. Guo, Y.; Zhang, X.; Zhang, X.; You, T., Defect- and S-rich ultrathin MoS₂ nanosheet embedded N-doped carbon nanofibers for efficient hydrogen evolution. *Journal of Materials Chemistry A* **2015**, *3* (31), 15927-15934.

123. Zhu, H.; Du, M.; Zhang, M.; Zou, M.; Yang, T.; Wang, S.; Yao, J.; Guo, B., S-rich single-layered MoS₂ nanoplates embedded in N-doped carbon nanofibers: efficient co-electrocatalysts for the hydrogen evolution reaction. *Chemical Communications* **2014**, *50* (97), 15435-15438.

124. Yan, Y.; Xia, B.; Li, N.; Xu, Z.; Fisher, A.; Wang, X., Vertically oriented MoS₂ and WS₂ nanosheets directly grown on carbon cloth as efficient and stable 3-dimensional hydrogen-evolving cathodes. *Journal of Materials Chemistry A* **2015**, *3* (1), 131-135.

125. Choi, Y.-H.; Lee, J.; Parija, A.; Cho, J.; Verkhoturov, S. V.; Al-Hashimi, M.; Fang, L.; Banerjee, S., An In Situ Sulfidation Approach for the Integration of MoS₂ Nanosheets on Carbon Fiber Paper and the Modulation of Its Electrocatalytic Activity by Interfacing with nC60. *ACS Catalysis* **2016**, *6* (9), 6246-6254.

126. Huang, H.; Huang, W.; Yang, Z.; Huang, J.; Lin, J.; Liu, W.; Liu, Y., Strongly coupled MoS₂ nanoflake-carbon nanotube nanocomposite as an excellent electrocatalyst for hydrogen evolution reaction. *Journal of Materials Chemistry A* **2017**, *5* (4), 1558-1566.

127. Liao, L.; Zhu, J.; Bian, X.; Zhu, L.; Scanlon, M. D.; Girault, H. H.; Liu, B., MoS₂ Formed on Mesoporous Graphene as a Highly Active Catalyst for Hydrogen Evolution. *Advanced Functional Materials* **2013**, *23* (42), 5326-5333.

128. Behranginia, A.; Asadi, M.; Liu, C.; Yasaei, P.; Kumar, B.; Phillips, P.; Foroozan, T.; Waranius, J. C.; Kim, K.; Abiade, J.; Klie, R. F.; Curtiss, L. A.; Salehi-Khojin, A., Highly Efficient Hydrogen Evolution Reaction Using Crystalline Layered Three-Dimensional Molybdenum Disulfides Grown on Graphene Film. *Chemistry of Materials* **2016**, *28* (2), 549-555.

129. Li, S.; Wang, S.; Salamone, M. M.; Robertson, A. W.; Nayak, S.; Kim, H.; Tsang, S. C. E.; Pasta, M.; Warner, J. H., Edge-Enriched 2D MoS₂ Thin Films Grown by Chemical Vapor Deposition for Enhanced Catalytic Performance. *ACS Catalysis* **2017**, *7* (1), 877-886.

130. Li, Y.; Wang, H.; Xie, L.; Liang, Y.; Hong, G.; Dai, H., MoS₂ Nanoparticles Grown on Graphene: An Advanced Catalyst for the Hydrogen Evolution Reaction. *Journal of the American Chemical Society* **2011**, *133* (19), 7296-7299.

131. Lu, Z.; Zhu, W.; Yu, X.; Zhang, H.; Li, Y.; Sun, X.; Wang, X.; Wang, H.; Wang, J.; Luo, J.; Lei, X.; Jiang, L., Ultrahigh Hydrogen Evolution Performance of Under-Water "Superaerophobic" MoS₂ Nanostructured Electrodes. *Advanced Materials* **2014**, *26* (17), 2683-2687.

132. Hinnemann, B.; Moses, P. G.; Bonde, J.; Jørgensen, K. P.; Nielsen, J. H.; Horch, S.; Chorkendorff, I.; Nørskov, J. K., Biomimetic Hydrogen Evolution: MoS₂ Nanoparticles as Catalyst for Hydrogen Evolution. *Journal of the American Chemical Society* **2005**, *127* (15), 5308-5309.

133. Jaramillo, T.; Jørgensen, K.; Lindner Bonde, J.; Nielsen, J.; Horch, S.; Chorkendorff, I., Identification of Active Edge Sites for Electrochemical H₂ Evolution from MoS₂ Nanocatalysts. *Science (New York, N.Y.)* **2007**, *317*, 100-2.

134. Benck, J. D.; Hellstern, T. R.; Kibsgaard, J.; Chakthranont, P.; Jaramillo, T. F., Catalyzing the Hydrogen Evolution Reaction (HER) with Molybdenum Sulfide Nanomaterials. *ACS Catalysis* **2014**, *4* (11), 3957-3971.

135. Kim, K. Y.; Lee, J.; Kang, S.; Son, Y.-W.; Jang, H. W.; Kang, Y.; Han, S., Role of Hyper-Reduced States in Hydrogen Evolution Reaction at Sulfur Vacancy in MoS₂. *ACS Catalysis* **2018**, *8* (5), 4508-4515.

136. Tang, Q.; Jiang, D.-e., Mechanism of Hydrogen Evolution Reaction on 1T-MoS₂ from First Principles.

ACS Catalysis **2016**, *6* (8), 4953-4961.

137. Zhang, T.; Zhu, H.; Guo, C.; Cao, S.; Wu, C.-M. L.; Wang, Z.; Lu, X., Theoretical investigation on the hydrogen evolution reaction mechanism at MoS₂ heterostructures: the essential role of the 1T/2H phase interface. *Catalysis Science & Technology* **2020**, *10* (2), 458-465.

138. Zhao, N.; Wang, L.; Zhang, Z.; Li, Y., Activating the MoS₂ Basal Planes for Electrocatalytic Hydrogen Evolution by 2H/1T' Structural Interfaces. *ACS Applied Materials & Interfaces* **2019**, *11* (45), 42014-42020.

139. Hu, J.; Zhang, C.; Yang, P.; Xiao, J.; Deng, T.; Liu, Z.; Huang, B.; Leung, M. K. H.; Yang, S., Kinetic-Oriented Construction of MoS₂ Synergistic Interface to Boost pH-Universal Hydrogen Evolution. *Advanced Functional Materials* **2020**, *30* (6), 1908520.

140. Wang, G.; Tao, J.; Zhang, Y.; Wang, S.; Yan, X.; Liu, C.; Hu, F.; He, Z.; Zuo, Z.; Yang, X., Engineering Two-Dimensional Mass-Transport Channels of the MoS₂ Nanocatalyst toward Improved Hydrogen Evolution Performance. *ACS Applied Materials & Interfaces* **2018**, *10* (30), 25409-25414.

141. Seh, Z. W.; Kibsgaard, J.; Dickens, C. F.; Chorkendorff, I.; Nørskov, J. K.; Jaramillo, T. F., Combining theory and experiment in electrocatalysis: Insights into materials design. *Science* **2017**, *355* (6321).

142. Escalera-López, D.; Griffin, R.; Isaacs, M.; Wilson, K.; Palmer, R. E.; Rees, N. V., MoS₂ and WS₂ nanocone arrays: Impact of surface topography on the hydrogen evolution electrocatalytic activity and mass transport. *Applied Materials Today* **2018**, *11*, 70-81.

143. Lassalle-Kaiser, B.; Merki, D.; Vrubel, H.; Gul, S.; Yachandra, V. K.; Hu, X.; Yano, J., Evidence from in situ X-ray absorption spectroscopy for the involvement of terminal disulfide in the reduction of protons by an amorphous molybdenum sulfide electrocatalyst. *Journal of the American Chemical Society* **2015**, *137* (1), 314-321.